INFORMATION TO USERS

This manuscript has been reproduced from the microfilm master. UMI films the text directly from the original or copy submitted. Thus, some thesis and dissertation copies are in typewriter face, while others may be from any type of computer printer.

The quality of this reproduction is dependent upon the quality of the copy submitted. Broken or indistinct print, colored or poor quality illustrations and photographs, print bleedthrough, substandard margins, and improper alignment can adversely affect reproduction.

In the unlikely event that the author did not send UMI a complete manuscript and there are missing pages, these will be noted. Also, if unauthorized copyright material had to be removed, a note will indicate the deletion.

Oversize materials (e.g., maps, drawings, charts) are reproduced by sectioning the original, beginning at the upper left-hand corner and continuing from left to right in equal sections with small overlaps.

Photographs included in the original manuscript have been reproduced xerographically in this copy. Higher quality 6" x 9" black and white photographic prints are available for any photographs or illustrations appearing in this copy for an additional charge. Contact UMI directly to order.

Bell & Howell Information and Learning
300 North Zeeb Road, Ann Arbor, MI 48106-1346 USA
800-521-0600

INVESTIGATION OF THE MECHANISMS CONTROLLING CHROMATE AND ARSENATE REMOVAL FROM WATER USING ZEROVALENT IRON MEDIA

by

Nikos T. Melitas

A Dissertation Submitted to the Faculty of the

DEPARTMENT OF CHEMICAL AND ENVIRONMENTAL ENGINEERING

In Partial Fulfillment of the Requirements
For the Degree of

DOCTOR OF PHILOSOPHY
WITH MAJOR IN ENVIRONMENTAL ENGINEERING

In the Graduate College

THE UNIVERSITY OF ARIZONA

2002

THE UNIVERSITY OF ARIZONA ®
GRADUATE COLLEGE

As members of the Final Examination Committee, we certify that we have read the dissertation prepared by Nikos T. Melitas

entitled Investigation of the Mechanisms Controlling Chromate and Arsenate Removal from Water Using Zerovalent Iron Media.

and recommend that it be accepted as fulfilling the dissertation requirement for the Degree of Doctor of Philosophy

Robert Arnold	3 June 02
Wendell Ela	06/03/02
James Farrell	6/03/02
	Date
	Date

Final approval and acceptance of this dissertation is contingent upon the candidate's submission of the final copy of the dissertation to the Graduate College.

I hereby certify that I have read this dissertation prepared under my direction and recommend that it be accepted as fulfilling the dissertation requirement.

James Farrell — Dissertation Director

6/03/02 — Date

STATEMENT BY THE AUTHOR

This dissertation has been submitted in partial fulfillment of requirements for an advanced degree at The University of Arizona and is deposited in the University Library to be made available to borrowers under rules of the Library.

Brief quotations from this dissertation are allowable without special permission, provided that accurate acknowledgment of source is made. Requests for permission for extended quotation from or reproduction of this manuscript in whole or in part may be granted by the head of the major department or the Dean of the Graduate College when in his or her judgment the proposed use of the material is in the interests of scholarship. In all other instances, however, permission must be obtained from the author.

SIGNED: 

ACKNOWLEDGEMENTS

I would like to thank my advisor, Professor James Farrell. Professor Farrell's excellent guidance and support has made my graduate study a great life experience. Professor Farrell has been more than an academic advisor; he has been a friend. Thanks to Professors Robert Arnold, Wendell Ela, Raymond Sierka and Ron LeBlank for creating a wonderful environment in the Environmental Engineering department. Special thanks to my colleagues Tie Li, Ouatfa Shuffe-Moscoso, Jianping Wang, Mark Kason, Ben Hauk and David Grassian. Thank you Trish for your great support.

DEDICATION

To my parents Theodore and Helen Melitas for their faith in me.

TABLE OF CONTENTS

TABLE OF CONTENTS - *continued*

TABLE OF CONTENTS – *continued*

LIST OF ILLUSTRATIONS

LIST OF ILLUSTRATIONS - *continued*

LIST OF ILLUSTRATIONS - *continued*

LIST OF ILLUSTRATIONS - *continued*

LIST OF TABLES

ABSTRACT

This research investigated the mechanisms controlling chromate and arsenate removal by zerovalent iron media. The removal kinetics of aqueous Cr(VI) and As(V) were studied in batch experiments for initial concentrations ranging from 100 to 10,000 μg/L. Removal kinetics were also studied in columns packed with zerovalent iron filings over this same concentration range. Electrochemical analyses were used to investigate the electron transfer reactions occurring on the iron surface, and to determine the effect of chromate and arsenate on the iron corrosion behavior.

The removal mechanism for chromate involved reduction to Cr(III) and the formation of hydroxide precipitates. Increasing chromate concentrations resulted in decreasing removal rates due to iron surface passivation. Even at low concentrations, chromate acts as a corrosion inhibitor and decreases iron corrosion rates. The condition of the iron surface prior to exposure to chromate determined the chromium removal kinetics. Air-formed oxides significantly inhibited chromate removal, whereas oxides formed in anaerobic, chromate-free water resulted in higher removal rates. Although direct reduction of chromate at cathodic sites on the iron surface was observed at early elapsed times, chromate removal eventually became limited by the rate at which Fe^{2+} could be generated at anodic sites.

The removal mechanism for arsenate did not involve reduction and was due to the formation of inner-sphere, bidentate complexes with iron corrosion products. At low arsenate concentrations the rate of arsenate removal was limited by diffusion to adsorption sites. At high concentrations the rate of arsenate removal was limited by the

rate of adsorption site generation resulting from iron corrosion. Adsorbed arsenate blocked electroactive sites on the iron surface and decreased iron corrosion rates. Arsenate is expected to remain as the principal adsorbed species in iron filter media because electrochemical reduction of As(V) to As(III) is not favorable under the conditions relevant to freely corroding iron.

CHAPTER 1

INTRODUCTION

1.1 Outline

Following this outline are a background section and a section providing the context for the research that was performed. The background section focuses on the sources, chemistry, health effects, and existing remediation technologies for removing chromium and arsenic compounds from water supplies. More specific information such as the findings of previous investigators, specific reactions, and background material on electrochemistry is included in the following chapters and is omitted from this to avoid redundancy. Chapters 2, 4, and 5 have been published in the journal *Environmental Science and Technology* (*1*, 2, 3). Chapter 3 is currently in review at that journal. Chapter 2 describes the effects of chromium concentration on its removal kinetics and on the corrosion behavior of zerovalent iron. Chapter 3 describes the effect of the initial condition of the iron surface on the kinetics of chromate removal. Chapter 4 consists of an investigation on the kinetics of arsenate removal by zerovalent iron, and the effect of arsenate concentration on the iron corrosion behavior. Chapter five describes an investigation on the electrochemical reactions that occur on the surface of zerovalent iron media in arsenate solutions. Chapter 6 is the final chapter that summarizes the major findings of this research.

1.2 Introduction

According to the National Priorities List developed by the United States Environmental Protection Agency (EPA), there are approximately 1000 contaminated sites in the United States that present significant environmental problems (*4*). Approximately 500 of these 1000 contaminated sites have elevated concentrations of toxic metals (*4*). Chromium and arsenic are the second and third most common metals, respectively, with 306 sites contaminated with chromium, and 235 sites contaminated with arsenic (*4*). In addition to its presence at industrially contaminated sites, arsenic presents a wider problem due to its natural abundance in the environment. High concentrations of arsenic have been found in drinking water supplies in developing countries such as Bangladesh and India (*5*). Additionally, arsenic contamination of drinking water is a problem in the western United States (*5*). Currently, the EPA has set a Maximum Contaminant Level (MCL) of 50 μg/L for chromium, and 10 μg/L for arsenic in drinking water.

1.2.1 Arsenic

Arsenic is an abundant element in nature and is present in more than 200 mineral species (*5*). Natural sources of arsenic include the leaching of arsenic containing minerals, and atmospheric deposition arising from volcanic activity. Mining, burning of fossil fuels, wood preservation, and arsenical pesticides are the major anthropogenic sources of arsenic in the environment.

Under conditions relevant to potable water supplies, arsenic exists in both the +5 and +3 oxidation states. The +5 oxidation state is known as arsenate, and the +3 oxidation state is called arsenite. The dominant arsenate and arsenite species depend on the pH value of the water. Table 1 lists the arsenate and arsenite species and the pK_a value for each species.

Both arsenate and arsenite are toxic and carcinogenic to humans and animals. Arsenic can cause gastrointestinal, cardiovascular and nervous system anomalies. Long-term exposure to arsenic is related with skin, lung, bladder and kidney cancers (*6*).

Commonly used arsenic removal processes for drinking water are chemical precipitation, coagulation/filtration, membrane filtration, lime softening, adsorption and ion exchange. Coagulation/filtration is most suitable for large water systems, whereas membrane and adsorption processes are more suitable for small water systems.

Arsenic removal by coagulation/filtration occurs by the addition of alum or ferric salts. These salts form insoluble metal hydroxides that adsorb and/or coprecipitate with arsenic. The resulting precipitates are then removed from the water by sedimentation and filtration. Arsenic removal levels greater than 90% can be achieved with high coagulant dosages (*5*). However, removal is highly dependent on pH (*5*). The presence of competing ions does not severely affect the removal efficiency.

Activated alumina has a high specificity for As(V) but is much less effective for removing As(III) due to competition by other adsorbing anions (*5*). Optimum adsorption occurs at pH values between 5.5 and 6, and is expected to significantly decline at values above 8.2, which is the point of zero charge for alumina (*5*).

Anion exchange processes can remove arsenic to concentrations below 5 μg/L. The major disadvantage of anion exchange is its low specificity for arsenic. Therefore, in the presence of other competing anions, the removal efficiency is significantly reduced. Removal is not sensitive to pH between 6.5 and 9 but it rapidly decreases outside this pH range (*5*).

Membrane processes, especially nanofiltration and reverse osmosis, can be very effective and remove more than 95% of dissolved arsenic compounds. However, fouling due to the presence of organics, particulates and dissolved constituents is a major concern and pre-treatment of water is usually required.

The recent decrease in the MCL for arsenic has stimulated the development of new cost effective technologies that can be used by small water systems. These technologies include iron oxide coated sand, granular ferric hydroxide (GFH), and zerovalent iron (*5*).

Iron oxide coated sand consists of sand grains covered with ferric hydroxide. This technology is based on the high affinity of ferric hydroxide for arsenic compounds. Several studies have shown that iron oxide coated sand can be effective for arsenic removal; however, the presence of competing ions and pH can significantly affect the system performance (*5*). Regeneration of the bed is not efficient due to the high stability of the adsorbed arsenic on the surface of the iron (*5*).

GFH is composed of poorly crystallized β-FeOOH. Field studies have shown GFH to be very effective for arsenic removal, outperforming activated alumina (*5*). Competition of sulfate with arsenate adsorption is not significant. In contrast, phosphate competes

strongly with arsenate for adsorption sites. GFH can be cost-effective due to its high adsorption capacity for both As(V) and As(III) (*5*).

Zerovalent iron (ZVI) fillings are being used in Bangladesh and India for the removal of arsenic from drinking water. Arsenic removal by ZVI is accomplished by adsorption of arsenic on the solid corrosion products (*7*). In the United States, column studies have shown that ZVI can effectively remove arsenic for extended periods of time (*8*, *9*).

1.2.2 Chromium

Chromium is commonly used as a corrosion inhibitor and is also used in the electroplating, textile manufacturing, leather tanning, pigment manufacturing, and wood preservation industries. Due to improper disposal from the aforementioned industries, chromium is a ubiquitous contaminant of soils and groundwater.

Under environmentally relevant conditions, chromium is commonly found in water in its +6 oxidation state as chromate, and in its +3 oxidation state as chromite. The dominant Cr(III) and Cr(VI) species depend on the pH value of the water. Table 2 lists the chromate and chromite species and their pK_a values. Because Cr(III) has a very low water solubility at neutral pH values, reduction of Cr(VI) to Cr(III) can be exploited as a chromium removal mechanism.

Hexavalent chromium is carcinogenic to both humans and animals. It is also acutely toxic and may cause liver and kidney damage, internal hemorrhages, and respiratory problems (*10*). Chronic exposure can cause dermatitis and skin ulcerations (*10*). Due to its high solubility and adverse health effects, Cr(VI) poses a significant environmental

hazard. In contrast, Cr(III) is an essential nutrient and is generally nontoxic at exposure levels found in water supplies (*10*).

Commonly employed technologies for removing chromium compounds from water include chemical precipitation, ion exchange, and membrane separations. Chemical precipitation is based on the reduction of soluble Cr(VI) to insoluble Cr(III) by the addition of a reductant, often ferrous ions. This process may require adjustment of the pH and can achieve removal efficiencies greater than 95% (*11*). Ion exchange can be a very effective method for chromium removal since chromate is often favored by exchange media over other common anions (*11*). Membrane separations for chromium removal include reverse osmosis and electrodialysis. In electrodialysis, chromate is electrochemically transported through an anion selective membrane as a result of an applied direct electric current. Both ion exchange and membrane methods produce a secondary, more concentrated waste stream that must be treated before disposal.

1.3 Research Motivation

Zerovalent iron has received considerable attention in recent years as a treatment medium for groundwater contaminated by chlorinated organic solvents and regulated metals. Permeable reactive barriers containing zerovalent iron fillings have been employed at more than 100 sites in the United States for the remediation of chlorinated organic compounds, inorganic anions, and metals. The advantage of passive *in situ* treatment using ZVI is the low operation and maintenance costs once the system has been installed. A schematic diagram of a permeable reactive barrier is shown in Figure 1.1. In

addition to its use in underground barriers, ZVI can also be utilized as a filter medium in above ground canister configurations, as shown in Figure 1.2.

Although several field and laboratory studies have shown the effectiveness of ZVI for removing chromium and arsenic compounds, the mechanisms controlling contaminant removal and the long-term effectiveness of the iron media have not been sufficiently investigated. A better understanding of the removal mechanisms can lead not only to better designs of existing remedial systems, but also to the development of new and more effective remedial technologies. The purpose of this work was to investigate the mechanisms and rate limiting factors for chromium and arsenic removal by zerovalent iron media.

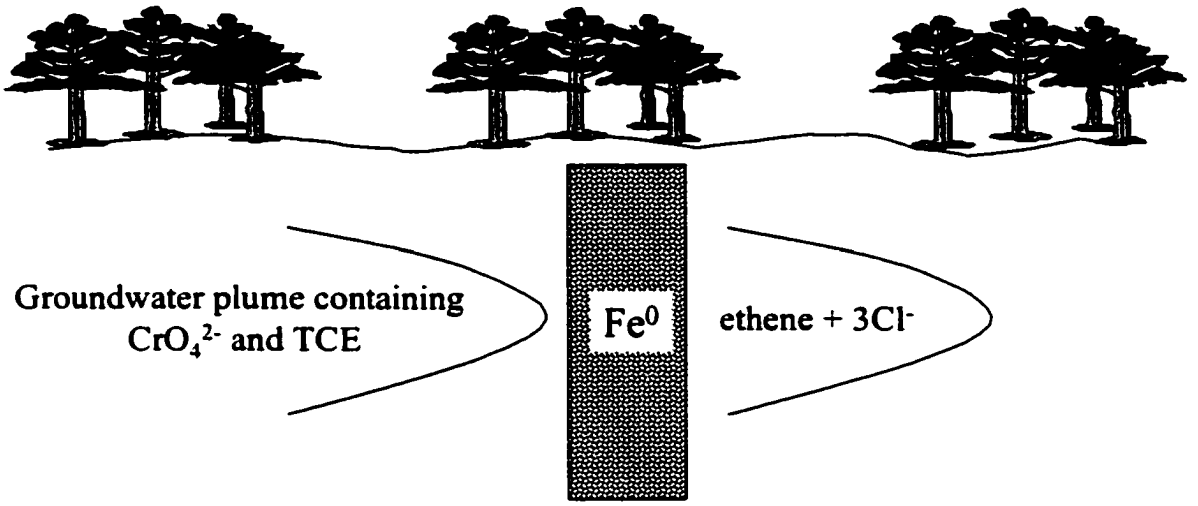

$$Fe^0 + CrO_4^{2-} + 4\ H_2O \rightarrow (Fe_xCr_{1-x})(OH)_3 + 2\ OH^-$$

$$Fe^0 + TCE + 3\ H^+ \rightarrow \text{ethene} + 3Cl^- + 3Fe^{2+}$$

Figure 1.1 Remediation of contaminated groundwater containing trichloroethylene (TCE) and chromate (CrO_4^{2-}) using ZVI reactive barrier. The reactive barrier intercepts the contaminated plume and TCE is reduced to ethane and chloride while chromate is reduced and precipitated as Cr(III) inside the barrier.

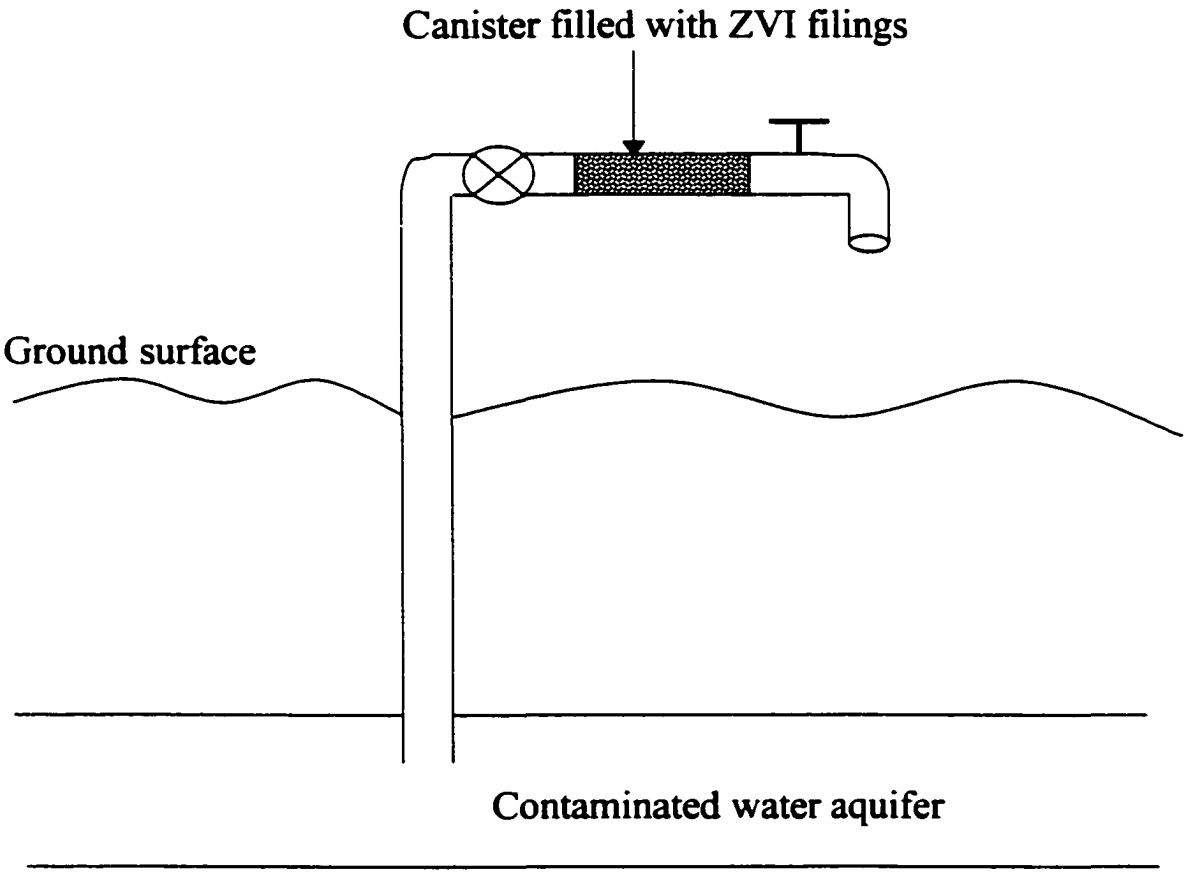

Figure 1.2 Canister filled with zerovalent iron filings is fitted into a well-head for the remediation of extracted drinking water.

CHAPTER 2

KINETICS OF SOLUBLE CHROMIUM REMOVAL FROM CONTAMINATED WATER BY ZEROVALENT IRON MEDIA: CORROSION INHIBITION AND PASSIVE OXIDE EFFECTS

2.1 Abstract

Permeable reactive barriers containing zerovalent iron are being increasingly employed for in situ remediation of groundwater contaminated with redox active metals and chlorinated organic compounds. This research investigated the effect of chromate concentration on its removal from solution by zerovalent iron. Removal rates of aqueous Cr(VI) by iron wires were measured in batch experiments for initial chromium concentrations ranging from 100 to 10,000 μg/L. Chromate removal was also measured in columns packed with zerovalent iron filings over this same concentration range. Electrochemical measurements were made to determine the free corrosion potential and corrosion rate of the iron reactants. In both the batch and column reactors, absolute rates of chromium removal declined with increasing chromate concentration. Corrosion current measurements indicated that the rate of iron corrosion decreased with increasing Cr(VI) concentrations between 0 and 5,000 μg/L. At a Cr(VI) concentration of 10,000 μg/L, Tafel polarization diagrams showed that chromium removal was affected by its diffusion rate through a passivating oxide film, and by the ability of iron to release Fe^{2+} at anodic sites. In contrast, water reduction was not mass transfer limited, but chromium did decrease the exchange current for the hydrogen evolution reaction. Even at the most passivating concentration of 10,000 μg/L, effluent Cr(VI) concentrations in the column

reactors reached a steady state, indicating that passivation had also reached a steady state. Although chromate contributes to iron surface passivation, the removal rates are still sufficiently fast for in situ iron barriers to be effective for Cr(VI) removal at most environmentally relevant concentrations.

2.2 Introduction

Chromium is one of the most common groundwater contaminants at industrial sites and military facilities due to its widespread use as a metal corrosion inhibitor (*12*). In recent years, there has been great interest in using permeable reactive barriers containing zerovalent iron for in situ treatment of groundwater contaminated with chlorinated organic compounds and redox active metals (*13*). For remediating redox active metals, the iron serves as an electron donor to reduce dissolved metal ions to valence states that are less water soluble. To date, more than 32 permeable barriers have been installed for groundwater remediation in the United States and Canada (*14*).

Previous investigators have shown that highly water soluble Cr(VI) may be removed from solution via reduction to Cr(III) according to (*15-20*):

$$Fe^0 + CrO_4^{2-} + 4H_2O = Cr(OH)_3 + Fe(OH)_3 + 2OH^- \qquad (1)$$

In addition to precipitation of $Cr(OH)_{3(s)}$, Cr(III) may also form $Cr_2O_{3(s)}$, or solid solutions with Fe(III) according to (*15, 16, 18*):

$$x\,Fe(OH)_3 + (1-x)\,Cr(OH)_3 = (Fe_xCr_{1-x})(OH)_3 \qquad (2)$$

where x can range from 0 to 1. In addition to reduction by zerovalent iron, Cr(VI) may also be reduced by atomic hydrogen adsorbed to iron surfaces (*15, 21, 22*), by Fe(II) in solution (*22-27*) or in mineral phases *(28-32*), or by dissolved organic compounds (*33, 34*).

Soluble chromate removal by zerovalent iron media has been described by a kinetic expression of the form (*22*):

$$\frac{d\{Cr(VI)\}}{dt} = -k\,A\,\{Cr(VI)\}^{0.5}\{H^{+}\}^{0.5} \qquad (3)$$

where, {Cr(VI)} is the aqueous chromate activity, k is the reaction rate constant, and A is the reactive surface area. The rate constant defined by equation 3 was found to depend on both the solution ionic strength and the mixing rate. Other investigators have found that chromate removal by iron media is dependent on the composition of the iron (*16*), and may also be affected by the presence of inorganic mineral phases that impact the solution chemistry (*15*).

The kinetic expression in equation 3 is 0.5 order in Cr(VI) concentration. Reaction orders less than unity are often indicative of reactive site saturation effects. However, in the case of zerovalent iron, the number and activity of the reactive sites is not fixed, and depends on both the iron and solution potentials. Therefore, the apparent 0.5 reaction order may be due to a rate limiting mechanism that involves electron transfer, and will thus be dependent on both the reactant concentration and the potential of iron.

The effect of potential and Cr(VI) concentration on the chromate reduction current (*12*) associated with a corroding iron electrode can be described by (*35*):

$$I = nFA\hat{k}\left[\{Cr(VI)\}e^{-\beta_c^{Cr}(E_{corr}-E^0)} - \{Cr(III)\}e^{\beta_a^{Cr}(E_{corr}-E^o)}\right] \quad (4)$$

where, n is the number of electrons transferred; F is the Faraday constant; A is the reactive surface area; $\hat{k}$ is the standard rate constant; β_c^{Cr} and β_a^{Cr} are the cathodic and anodic Tafel slopes, respectively, for the Cr(VI)/Cr(III) redox couple; E^o is the standard reduction potential for the Cr(VI)/Cr(III) redox couple; E_{corr} is the free corrosion potential; and {Cr(VI)} and {Cr(III)} are the activities of the Cr(VI) and Cr(III) species, respectively. The standard rate constant is independent of potential, and depends only on the kinetic facility of the redox reaction on the surface of interest (*35*).

Field studies have demonstrated that permeable iron barriers are effective for Cr(VI) removal over extended periods of operation *(36-38)*. However, chromate is a strong oxidant and is a well-known passivator of iron (*21*). Therefore, the buildup of chromium compounds on the iron surfaces may decrease reaction rates for chromate removal. This research investigated the hypothesis that increasing concentrations of chromate may contribute to decreasing reaction rates through increased surface passivation. The specific objectives of this investigation were to determine the effect of the Cr(VI) concentration on its removal rate, and on the corrosion rate of the zerovalent iron.

2.3 Materials and Methods

2.3.1 Batch Reactors

Batch experiments measuring soluble Cr(VI) removal by iron wires were performed in well-stirred, sealed 0.85 L glass reactors containing potassium chromate in 3 mM $CaSO_4$ background electrolyte solutions. In experiments measuring Cr(VI) removal rates, a

single 10 cm long by 1.2 mm diameter iron wire of 99.9% purity (Aesar, Ward Hill, MA) was used as the reactant. Anaerobic conditions were maintained by purging the reactors with humidified nitrogen gas. Samples were taken using a 1 mL glass syringe, with and without 0.1 μm nylon syringe filters (Whatman, Clifton, NJ). In all experiments, solution pH values were measured with color-calibrated test strips, and aqueous chromium concentrations were determined using a Perkin Elmer (San Jose, CA) model 4110zL graphite furnace atomic absorption spectrophotometer.

2.3.2 Packed Column Experiments

Column experiments were performed using either a 50 cm long by 2.5 cm outer diameter (o.d.) glass column, or a 25 cm long by 0.9 cm o.d. stainless steel column. Both columns were packed with Master Builder's Supply (Cleveland, OH) iron filings GX-27 blend. The glass column contained three intracolumn sampling ports at 12.5, 25, and 37.5 cm from the influent end. One port at each location served for taking aqueous samples and for measuring the redox potential of the solution. The other port was used to determine the free corrosion potential of the iron reactants. The corrosion potentials were measured using an iron wire permanently inserted into the column through a rubber septum at each port. The columns were operated with Cr(VI) concentrations ranging from 100 to 10,000 μg/L in 3 mM $CaSO_4$ background electrolyte solutions. The mean hydraulic residence time in the 25 cm column was 25 minutes, and was 19 minutes in the 50 cm column.

2.3.3 Electrochemical Experiments

Two types of electrochemical experiments were performed to assess the effect of chromate concentration on iron corrosion rates. To assess the effect of concentration on initial rates of iron corrosion, a single 10 cm long iron wire was placed in 0.75 L of 3 mM $CaSO_4$ electrolyte solution in one of the glass reactors containing a calomel reference electrode and a stainless steel counter electrode. The solution was continuously purged with 50 mL/min of humidified nitrogen gas, and potassium chromate was added to the reactor through the vent tubing to produce dissolved chromium concentrations ranging from 100 to 10,000 μg/L. The wire was exposed to each concentration for 1 day, at which point a Tafel scan was performed.

To determine the effect of elapsed time on iron corrosion rates in solutions of approximately constant chromium concentration, 2.6 cm long iron wires were placed in the nitrogen-purged, glass reactors containing Cr(VI) at concentrations of 0, 100, 5,000 or 10,000 μg/L. Short wires were used in order to minimize changes in solution concentration over the course of these experiments. Tafel scans were performed to measure changes in the corrosion currents and free corrosion potentials as a function of elapsed time.

All Tafel diagrams were produced by polarizing the wires ±200 mV with respect to their open circuit potentials (*39*). The polarization experiments were performed using an EG&G (Oak Ridge, TN) model 273A scanning potentiostat and M270 software. All potentials are reported with respect to the standard hydrogen electrode (SHE).

2.4 Results and Discussion

2.4.1 Removal Kinetics

Aqueous chromate concentrations in the batch reactors as a function of elapsed time are shown in Figure 1. Filtered and unfiltered samples gave similar results, indicating that the chromate removed from solution was associated with the iron wires. Comparison of chromium removal rates in stirred and unstirred reactors indicated that the observed rates were not significantly affected by hydrodynamic boundary layer mass transfer limitations. In all experiments, pH values remained constant at approximately 7. No detectable removal was observed in the reactor with an initial concentration of 10,000 μg/L. In the remaining reactors, the chromate removal kinetics could be adequately described by a zero order kinetic model, as illustrated in Figure 1. However, for initial concentrations between 100 and 5,000 μg/L, the observed removal rates decreased with increasing chromate concentration, as shown in Table 1.

The decreasing Cr(VI) removal rates with increasing concentration can be explained by lower rates of iron corrosion at higher chromate concentrations. Figure 2a shows the corrosion rate of a single iron wire exposed to increasing chromate concentrations for 1 day at each concentration. The higher corrosion potentials and lower corrosion currents observed with increasing concentration between 100 and 5,000 μg/L are indicative of the action of an oxidant/passivator like chromate (*39, 40*). As shown in Figure 2b, corrosion currents in the constant concentration reactors also decreased with increasing chromate concentration.

In contrast to many catalytic systems where the activity of the reactive sites is independent of the reactant concentration, the reactivity of sites on zerovalent iron may be expected to decline with increasing oxidant concentration. This can be attributed to the effect of potential on the rate of electrochemical reactions, and on the passivating effect of a corrosion inhibitor like chromate. As shown by the potential data in Figure 2a, between 100 and 5,000 μg/L, higher Cr(VI) concentrations resulted in higher E_{corr} values. According to equation 4, the rate of Cr(VI) reduction by zerovalent iron should be dependent on both the Cr(VI) concentration and the potential of the iron. However, the behavior predicted by equation 4 is not consistent with the results in Table 1. For example, using the measured cathodic Tafel slope for Cr(VI) reduction of 0.0049 dec/mV, and the potential data in Figure 2a, equation 4 predicts that the Cr(VI) removal rate at a concentration of 5,000 μg/L should be 44 times greater than that observed at a concentration of 100 μg/L. However, as shown in Table 1, the removal rate actually declined with increasing Cr(VI) concentration. This behavior can only be attributed to increasing iron surface passivation with increasing chromate concentration.

Iron surface passivation can be attributed to both anodic and cathodic inhibition of iron corrosion. The cathodic (I_c) and anodic (I_a) currents produced in the Tafel scans can be expressed as (*39*):

$$I_c = I_o^c e^{-\beta_c (E - E_{eq}^c)} \tag{5}$$

$$I_a = I_o^a e^{\beta_a (E - E_{eq}^a)} \tag{6}$$

where, I_o^a and I_o^c are the anodic and cathodic exchange currents, respectively, while E_{eq}^a and E_{eq}^c are the equilibrium potentials for the anodic and cathodic redox reactions. The exchange currents depend on the kinetic facility of the reaction, the reactant concentrations, and the surface area available for reduction or oxidation (*39*). Figure 3a compares Tafel diagrams generated in the blank and 100 µg/L solutions. The cathodic Tafel slopes of 0.0065 dec/mV in both solutions are similar to literature values for water reduction in neutral and alkaline media of 0.006 to 0.0072 dec/mV (*41-43*). This indicates that water was the primary oxidant in both solutions, and that the current associated with Cr(VI) reduction was too low to measurably contribute to the observed corrosion current.

Although the Tafel slopes shown in Figure 3a were similar in both solutions, there was lower current at each potential in the Cr(VI) containing reactor. As illustrated by equation 5, the lower cathodic current in the chromate reactor can be attributed to a factor of 2 decline in I_o^c for water reduction. This decrease in I_o^c for water can likely be attributed to the deposition of Cr(III) oxides at cathodic sites on the iron surface (*43, 44*). Spectroscopic analysis has found that both $Cr(OH)_3$ and Cr_2O_3 deposit at cathodic sites on iron surfaces (*18, 20, 43*). As illustrated by equation 6, the lower anodic current in the chromate versus the blank solution can be attributed to a decrease in I_o^a. This factor of 1.6 decline in current in the anodic Tafel region likely results from the presence of Fe(III) or mixed Cr(III)/Fe(III) oxides at anodic sites on the iron surface. These oxides decrease the surface area available for the anodic reaction of iron oxidation.

Figure 3b shows Tafel scans taken after one day elapsed for the iron wires immersed in the 5,000 and 10,000 μg/L Cr(VI) solutions. Comparison of the diagrams in Figures 3a and b show that the β_c values after one day elapsed decreased with increasing Cr(VI) concentration. This can be attributed to a decreasing contribution of water reduction to the total rate of iron corrosion. The inhibition of water reduction was caused by the increase in potential of the iron, and by a decrease in the I_o^c for water reduction. At a chromate concentration of 100 μg/L, the β_c of 0.0065 dec/mV indicates that water reduction was the primary cathodic reaction. However, inhibition of water reduction increased the contribution of other cathodic reactions to the observed corrosion current. At a concentration of 10,000 μg/L, reduction of chromate appears to be the dominant reaction contributing to iron corrosion after one day elapsed. The β_c of 0.0049 dec/mV in the 10,000 μg/L solution is close to the β_c of 0.0050 dec/mV observed by other investigators for a chromate-coated iron electrode immersed in a 780,000 μg/L Cr(VI) solution (*43*). Additionally, the potential in the 10,000 μg/L solution of –400 mV is close to the equilibrium potential for water reduction, indicating that there was minimal hydrogen evolution after one day elapsed. As shown in Figure 3b, the β_c of 0.0057 dec/mV in the 5,000 μg/L solution was intermediate to the β_c values in the blank and 10,000 μg/L reactors. This indicates that both water and chromate reduction contributed to the observed rate of iron corrosion at 5,000 μg/L.

Mass transfer limitations are evident in the cathodic Tafel slopes in the 10,000 μg/L solution. The flattening of the 10,000 μg/L cathodic Tafel slope in Figure 3b at a current of 1 μA was due to mass transfer effects. During the cathodic scan, reduction of Cr(VI)

decreased the chromate concentration in the vicinity of the cathodic sites. At a potential of –520 mV, the rate of reduction became faster than the rate of Cr(VI) diffusion to cathodic sites. This limited the reduction rate to the rate of chromate diffusion, and resulted in a cathodic mass transfer limited current (I^c_{lim}) of ~1 μA.

There was a gradual decline in I^c_{lim} at 10,000 μg/L with increasing elapsed time. Tafel scans for this reactor at 1, 18 and 37 days elapsed are compared in Figure 4. The I^c_{lim} values for Cr(VI) reduction declined from ~1 μA after one day elapsed to 0.4 μA after 37 days. This can be attributed to increasing mass transfer limitations for Cr(VI) reduction with elapsed time. However, the small difference in mass transfer limitations between 18 and 37 days suggests that the surface passivation was approaching a steady state.

The Cr(VI) concentration also affected the anodic Tafel slopes in each reactor. As illustrated by the β_a values in Figures 3a and b, increasing chromate concentrations resulted in decreasing anodic Tafel slopes for iron oxidation. Decreasing β_a values are indicative of increasing anodic inhibition of iron corrosion. This inhibition likely arises from formation of Fe(III) and Fe(III)/Cr(III) oxides produced via reaction of Cr(VI) with Fe^{2+} released at anodic sites (*15, 21*). These insoluble oxides decrease the rate that Fe^{2+} released at underlying anodic sites may enter the solution. The buildup of Fe^{2+} under the oxide layer leads to concentration polarization, and thereby reduces the thermodynamic favorability for further iron oxidation. This effect is essentially a mass transfer limitation on the iron oxidation reaction.

Although increasing cathodic inhibition was observed with elapsed time in Figure 4, there was decreasing anodic inhibition between 1 and 18 days elapsed. This decreasing anodic inhibition can be seen by the greater mass transfer limited current for iron oxidation (I^{a}_{lim}) at 18 days compared to that at 1 day. This type of behavior has been attributed to reductive dissolution of the iron oxide film, and to morphological changes in the oxides coating the iron (*45*). Changing oxide morphology can be seen in the Tafel slopes that occur after the mass transfer limited current for iron oxidation. The 1 and 18 day scans in Figure 4 show two additional anodic Tafel slopes, while the 37 day scan shows only one additional slope beyond that for iron oxidation. These additional slopes result from oxidation of different iron oxides (*43*). The fact that there was only one oxide Tafel slope at 37 days elapsed suggests that the oxide is more uniform at this time than at 1 and 18 days.

Changes in the oxide coating the iron are reflected in changes in electrode potential. The temporal oscillations in E_{corr} illustrated for the 10,000 μg/L reactor in Figure 4 were observed in all reactors. These potential oscillations are associated with oscillations in Cr(VI) removal rates, as illustrated in Figure 1 for the 400 and 1,700 μg/L reactors. Periods of declining potential are associated with faster removal rates, while periods of increasing potential are associated with slower removal rates.

2.4.2 Column Results

Results from a long-term column experiment measuring Cr(VI) removal rates as a function of influent concentration are shown in Figure 5. The influent Cr(VI)

concentrations for each period are summarized in Table 2. Influent and effluent pH values were always 7 ± 0.5. For influent Cr(VI) concentrations between 100 and 5,000 μg/L, effluent concentrations in the 25 cm column remained below the detection limit of 0.5 μg/L. This indicates that rates of Cr(VI) removal were too fast to be measured for influent concentrations between 100 and 5,000 μg/L. However, as shown in Figure 5, an influent concentration of 10,000 μg/L resulted in chromium breakthrough, with a steady state effluent concentration of ~7,000 μg/L. This steady state removal was observed for a period of 30 days (~1,700 pore volumes) until the experimental conditions were changed.

Upon lowering the influent concentration back to 1,000 μg/L at 252 days elapsed, the effluent concentration declined to a steady state value of ~200 μg/L. Previously, as shown in Table 2, an influent concentration of 1,000 μg/L resulted in complete chromium removal. Therefore, the greater effluent concentration between 252 and 267 days indicates that exposure of the iron to the 10,000 μg/L solution produced a loss in reactivity that resulted in slower rates of Cr(VI) removal. However, this loss in reactivity was slowly reversible. To investigate recovery in iron reactivity, the column was shut in between 267 and 274 days elapsed. Upon resuming flow at an influent concentration of 1,000 μg/L, the effluent concentration decreased to ~20 μg/L, as shown in Figure 5. This behavior indicates that the performance of zerovalent iron for Cr(VI) removal is hysteretic, and is highly dependent on the condition of the iron surfaces.

Data from the 50 cm glass column indicates that the condition of the iron surfaces varied with time and location along the length of the column. In all three sampling ports, the potential of the iron decreased with elapsed time until the chromate front reached that

port. Figure 6a shows the iron wire potential from the middle sampling port of the glass column, while Figures 6b and c show the solution potential (E_{aq}) and chromate concentration, respectively. During the period when there was complete chromate removal before sampling port 2, a continuous decrease in E_{corr} was observed after an initial potential fluctuation. This decreasing potential is consistent with the potential behavior in the batch experiments, and cannot be explained by changes in solution potential, since the solution potential increased monotonically with time. The potential fluctuations observed during the first 15 days elapsed can most likely be attributed to reduction of the air-formed oxide, and the subsequent formation of $Fe(OH)_2$ (*46*). The almost linear potential drop between 15 and 47 days elapsed can likely be attributed to transformation of $Fe(OH)_2$ to a porous layer of magnetite (Fe_3O_4), as observed by previous investigators (*46*).

Upon breakthrough, and exposure of the iron wire in the center port to chromate at 47 days elapsed, the potential sharply increased due to the oxidizing action of chromate, and the formation of passivating Fe(III)/Cr(III) oxides. The subsequent potential decline between 55 and 63 days elapsed can likely be attributed to reduction of the passive film (*45*). After 63 days elapsed, the potential gradually increased due to continuous exposure to high Cr(VI) concentrations, and the build-up of a chromium-enforced passive layer. Similar temporal oscillations in potential were observed for all three intracolumn iron wire probes, and in the batch experiments, as illustrated in Figure 4 for the 10,000 μg/L reactor.

Overall Cr(VI) removal in the 50 cm glass column was similar to that observed in the 25 cm column. As indicated in Table 3, feed concentrations less than 5,000 μg/L resulted in complete chromium removal before the first sampling port, and the first appearance of measurable chromium in the column effluent occurred at a feed concentration of 10,000 μg/L. Since measurable chromium concentrations were observed only for the two highest feed concentrations, Cr(VI) removal rates can be calculated only for influent concentrations of 5,000 and 10,000 μg/L. Mass balances on the column showed steady state removal rates of 707 and 36 μg/(L min) for influent concentrations of 5,000 μg/L and 10,000 μg/L, respectively. This decrease in removal rate with increased feed concentration is consistent with results of the batch tests, and illustrates that Cr(VI) removal kinetics cannot be described by simple zero, first, or fractional order kinetic models that do not account for iron surface passivation.

Even at the most passivating concentration of 10,000 μg/L, effluent chromate concentrations in both columns reached a steady state within several days. This indicates that the extent of surface passivation had also reached a steady state. Steady state performance may be attributed to continuous generation of new diffusion pathways and reaction sites arising from crack formation in the oxide layer. This is consistent with previous reports that only thin passive films may remain nonporous, since internal stresses lead to crack formation as the oxide film grows (*47, 48*).

Similar cathodic and anodic mass transfer limited currents at 37 days elapsed in the 10,000 μg/L solution indicate that chromium removal rates are affected by both the ability of Cr(VI) to penetrate passivating oxides, and by the ability of iron to release Fe^{2+}

at anodic sites. Although Cr(VI) concentrations as low as 100 μg/L significantly decrease corrosion rates, concentration increases above 1,000 μg/L have only a minimal effect on the rate of corrosion, despite significantly impacting the rate of Cr(VI) removal. This is consistent with an oxide film that acts as a diffusion barrier for Cr(VI) reduction. Since rates of Cr(VI) removal are limited by its mass transfer, and the mass transfer of Fe^{2+} ions through the oxide film, thicker films associated with higher Cr(VI) concentrations decrease the mass transfer rates, and thereby decrease chromate removal rates. In contrast, the Tafel scans indicate water reduction is not limited by mass transfer, and the effect of chromium on hydrogen evolution occurs via directly blocking cathodic sites. Therefore, the thickness of the oxide film has only a small impact on the rate of water reduction.

Although results from this research show that chromate contributes to iron surface passivation, the column results suggest that removal rates can reach steady state values that are sufficiently fast to provide effective removal for most environmentally relevant concentrations, which are often less than 10,000 μg/L (*14*). This is confirmed by field studies showing that permeable barriers containing zerovalent iron can reduce aqueous Cr(VI) concentrations to nondetectable levels (36, *37, 38*). For example, a permeable barrier operating at a flow velocity of ~50 cm per day has been effective for treating groundwater with Cr(VI) concentrations up to 10,000 μg/L for more than two years (*49, 50*). This indicates that for typical groundwater flow rates, diffusion of Cr(VI) and Fe^{2+} through the passivating films are sufficiently fast to provide for complete Cr(VI) removal. However, since chromate decreases iron corrosion rates, the presence of even

low levels of Cr(VI) may adversely affect treatment of other contaminants at sites where permeable barriers are used for remediating plumes containing both chromate and chlorinated organic compounds.

2.5 Acknowledgement

The authors thank Dr. Wayne Seames and Gina Bailey for their assistance. Although the research described in this article has been funded by the United States Environmental Protection Agency through grant R-825223-01-0 to J.F., it has not been subjected to the Agency's peer and policy review, and therefore does not necessarily reflect the views of the Agency, and no official endorsement should be inferred.

Table 2.1 Zero Order Rate Constants (k_o) with 95% Confidence Intervals for Chromate Removal from Solutions with Different Initial Cr(VI) Concentrations (C_o).

C_o (μg/L)	k_o (μg/m^{2}min)	Correlation Coefficient (R^2)
100	94±10	0.98
400	56±7	0.97
1,700	48±22	0.82
5,000	14±7	0.86

Table 2.2 Influent and Effluent Cr(VI) Concentrations for the 25 cm Column Operated with a Mean Hydraulic Detention Time of 25 Minutes.

Days Elapsed	Influent Concentration (μg/L)	Effluent Concentration (μg/L)
0-117	100	0
117-132	300	0
132-146	600	0
146-183	1,000	0
183-193	1,500	0
193-207	5,000	0
207-252	10,000	7,000
252-267	1,000	200
267-274	shut-in	shut-in
274-296	1,000	20

Table 2.3 Influent and Effluent Cr(VI) Concentrations for the 50 cm Column Operated with a Mean Hydraulic Detention Time of 19 Minutes.

Days Elapsed	Influent Concentration (μg/L)	Effluent Concentration (μg/L)
0-6	100	0
6-12	200	0
12-18	400	0
18-24	800	0
24-32	1,200	0
32-40	2,500	0
40-46	5,000	0[1]
46-122	10,000	9,100

[1]Steady state concentration of 580 μg/L was observed at port 1.

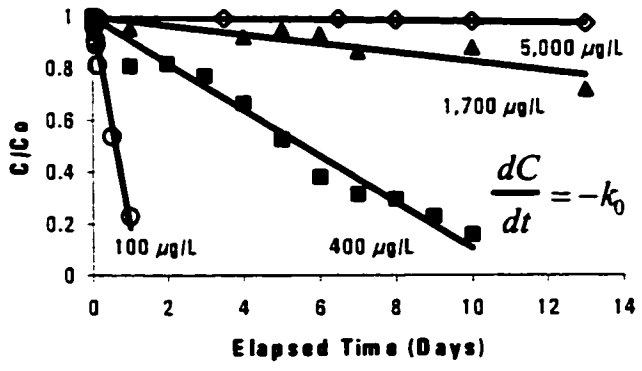

Figure 2.1 Aqueous Cr(VI) concentrations in the iron wire batch reactors with differing initial Cr(VI) concentrations. Zero order (k_o) removal rate constants for each initial concentration are presented in Table 1.

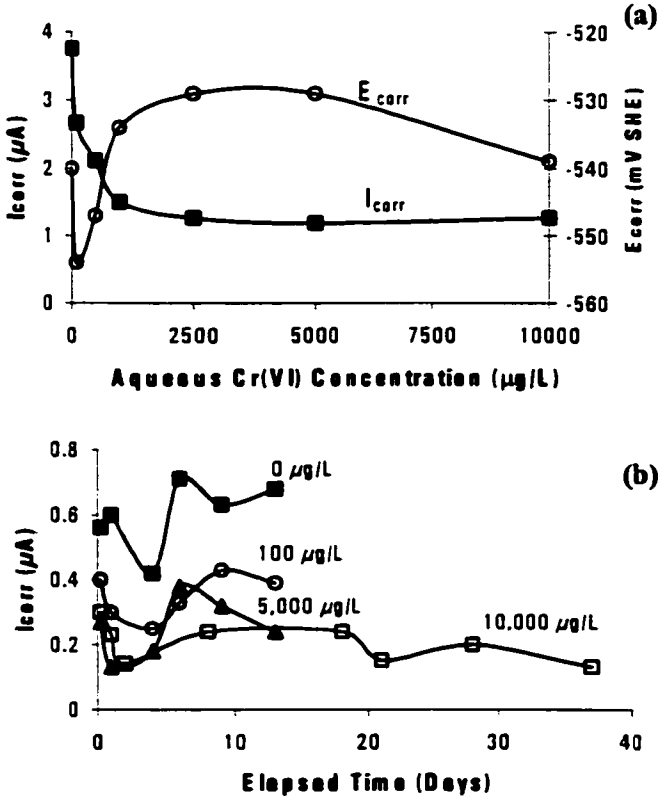

Figure 2.2 a) Corrosion currents (I_{corr}) and free corrosion potentials (E_{corr}) for a single 10 cm long iron wire immersed in anaerobic Cr(VI) solutions after one day elapsed at each concentration. The wire was exposed to each Cr(VI) concentration for 1 day before each measurement was taken. b) Corrosion currents for 2.6 cm long iron wires immersed in anaerobic solutions of different initial Cr(VI) concentration. In the 5,000 and 10,000 μg/L reactors, there was no measurable Cr(VI) removal over the duration of the current measurements.

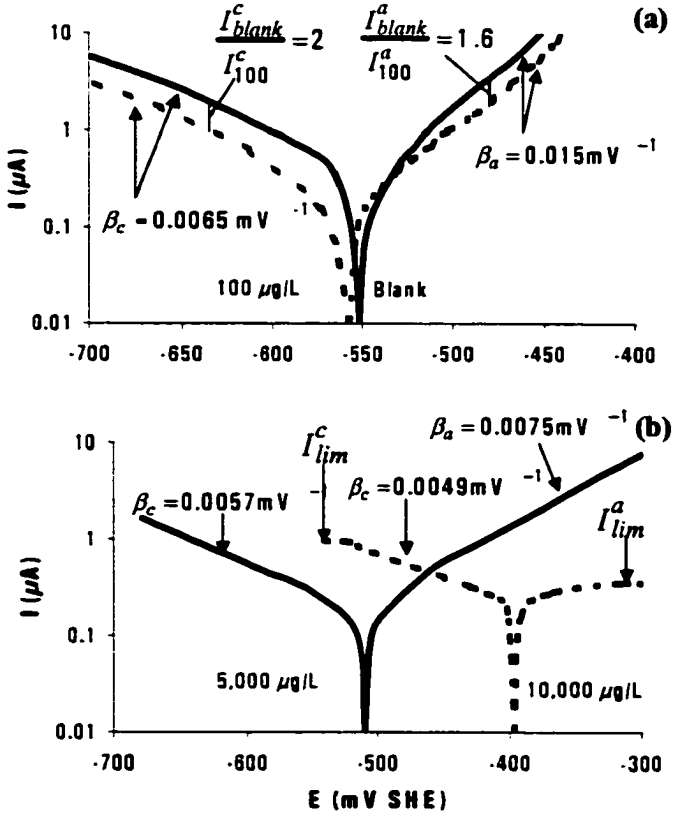

Figure 2.3 Tafel scans after 1 day elapsed for 2.6 cm long iron wires immersed in anaerobic 3 mM $CaSO_4$ background electrolyte solutions with initial Cr(VI) concentrations of: a) 0 and 100 µg/L; and b) 5,000 and 10,000 µg/L.

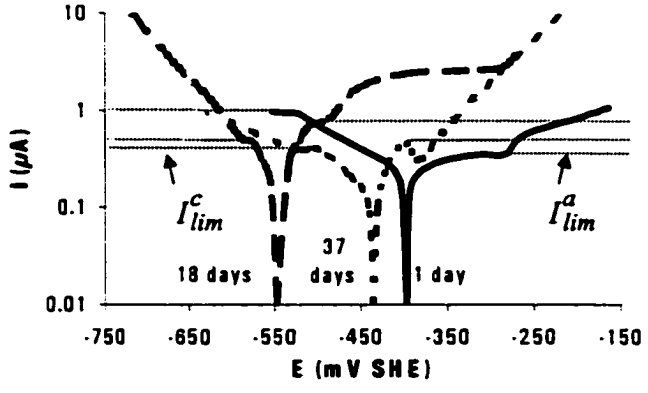

Figure 2.4 Tafel scans after 1, 18 and 37 days elapsed for a 2.6 cm long iron wire electrode immersed in an anaerobic 3 mM $CaSO_4$ background electrolyte solution with an initial Cr(VI) concentration of 10,000 μg/L.

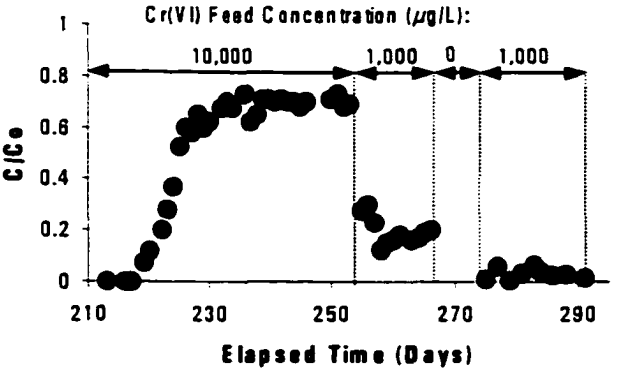

Figure 2.5 Effluent chromium concentrations as a function of elapsed time for a 25 cm long column packed with 40 g of iron filings and operated at Cr(VI) concentrations ranging from 100 to 10,000 μg/L in an anaerobic 3 mM $CaSO_4$ background electrolyte solution. Influent and effluent chromium concentrations for the entire experiment are listed in Table 2.

Figure 2.6 Data for a 50 cm long column packed with 323 g of iron filings and operated with influent Cr(VI) concentrations ranging from 100 to 10,000 μg/L in an anaerobic 3 mM $CaSO_4$ background electrolyte solution. Influent and effluent chromium concentrations for the entire experiment are listed in Table 3; a) E_{corr} values for an iron wire probe permanently inserted into the column at the middle sampling port; b) Solution potentials measured at the middle sampling port; and c) Aqueous chromium concentrations at the middle sampling port.

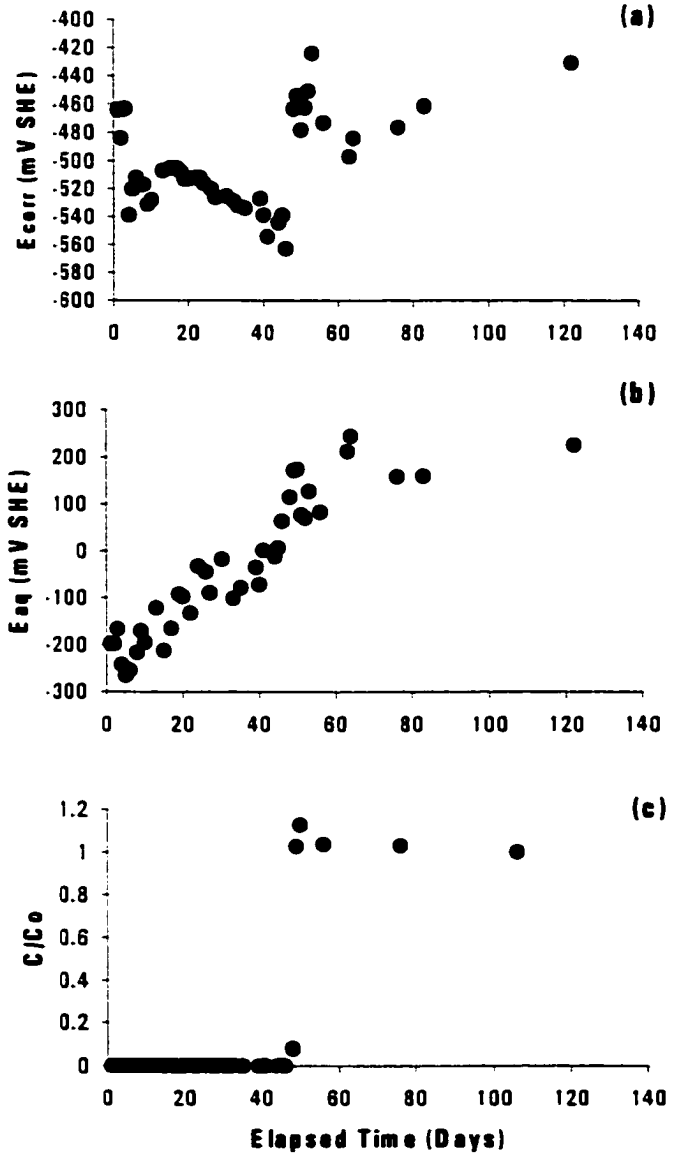
(a)
Ecorr (mV SHE)
-400
-420
-440
-460
-480
-500
-520
-540
-560
-580
-600
0
20
40
60
80
100
120
140
(b)
Eaq (mV SHE)
300
200
100
0
-100
-200
-300
0
20
40
60
80
100
120
140
(c)
C/Co
1.2
1
0.8
0.6
0.4
0.2
0
0
20
40
60
80
100
120
140
Elapsed Time (Days)

CHAPTER 3

UNDERSTANDING CHROMATE REACTION KINETICS WITH CORRODING IRON MEDIA USING TAFEL ANALYSIS AND ELECTROCHEMICAL IMPEDANCE SPECTROSCOPY

3.1 Abstract

The kinetics of chromate removal from contaminated water by zerovalent iron media are not well understood. This study investigated the reactions occurring on iron surfaces in chromate solutions in order to understand the removal kinetics and to assess the long-term ability of zerovalent iron for removing Cr(VI) from contaminated water. Tafel polarization analysis and electrochemical impedance spectroscopy were used to determine the corrosion rates and charge transfer resistances associated with Cr(VI) removal by iron wires suspended in electrolyte solutions with initial Cr(VI) concentrations of 10,000 μg/L. The condition of the iron surfaces at the time of their exposure to chromate determined the effectiveness of the iron for chromate removal. Both iron coated with a water-formed oxide and initially oxide-free iron were effective for chromate removal. However, iron coated with an air-formed oxide was an order of magnitude less effective for removing soluble chromium. Although iron with the air-formed oxide was largely passivated with respect to chromate removal, its overall rate of corrosion was similar to that for iron with the other initial surface conditions. This indicates that water, but not chromate, was able to penetrate the air-formed oxide coating and access cathodic sites. For all initial surface conditions, addition of chromate

decreased the corrosion rate by increasing the corrosion potential and the anodic charge transfer resistance. Although Cr(VI) is a strong oxidant, rates of iron corrosion were not proportional to the aqueous Cr(VI) concentrations due to anodic control of iron corrosion. Under anodically controlled conditions, the rate of corrosion was limited by the rate at which Fe^{2+} could be released at anodic sites, and not by the rate at which oxidants were able to accept electrons. This study shows that the zero order removal kinetics of Cr(VI) by iron media can be explained by anodic control of iron corrosion, and the concomitant anodic control of Cr(VI) reduction.

3.2 Introduction

Permeable reactive barriers containing zerovalent iron media are becoming increasingly employed for passive remediation of groundwater contaminated with hexavalent chromium compounds (*51*). Several investigators have reported that the removal mechanism involves reduction of highly soluble CrO_4^{2-} to sparingly soluble Cr(III) compounds at the surface of the iron (*52- 58*). Spectroscopic data has shown that $Cr(OH)_3$ and mixed Cr(III)/Fe(III) hydroxides are precipitated on the iron surface (*552, 553, 555, 557, 558*). Although both field and laboratory studies have shown that corroding iron media can be highly effective for chromate removal, the kinetics of the removal process are not well understood.

Rates of Cr(VI) removal from solution by zerovalent iron have generally been described by models of the form:

$$\frac{d[Cr(VI)]}{dt} = -k[Cr(VI)]^n \qquad (1)$$

where k is a rate constant that depends on the iron type and surface area, solution chemistry, and pH. The n parameter is the reaction order with respect to the aqueous Cr(VI) activity, [Cr(VI)]. In batch tests using iron wires as the reacting iron species, Gould (*59*) found that an n value of 0.5 best described initial removal rates. Other batch studies have reported both zeroth and first order removal kinetics for initial reaction rates (*552, 558, 60*), and that rates increasingly deviated from first order kinetics with increasing elapsed time (*558*). Deviations the first order kinetic model with time have been attributed to changes in iron reactivity associated with passivation by adsorbed Cr(III) compounds (*558, 60*).

An understanding of the steady state removal kinetics is needed in order to design permeable barriers for chromate removal. However, it is difficult to assess steady state rates of Cr(VI) removal using short-term batch tests. Studies using a large iron surface area with respect to the amount of soluble chromate utilize only a very small fraction of the reductive capacity of the iron. In fact, much of the removal in short-term batch tests may be attributable to adsorption on, or reduction by, oxides present on the iron at the time of its immersion into solution. Therefore, short-term tests exploiting only a small fraction of the iron's reactive capacity may not be representative of long-term performance where continous iron corrosion is necessary for sustained Cr(VI) removal. Another pitfall of batch testing with iron filings is that the vigorous mixing that is usually employed contributes to particle-particle collisions that may abrade passivating oxides off the iron surfaces.

In a previously reported investigation, Melitas et al. (*61*) used iron wires suspended in

chromate solutions to determine steady state removal rates, and to assess the effect of surface passivation on the long-term removal kinetics. A small reactive surface area and a large solution volume was employed in order to achieve high loadings of adsorbed Cr(III) compounds on the iron surfaces. For initial chromate concentrations ranging from 100 to 5,000 μg/L, steady state rates of Cr(VI) removal were observed to follow zeroth order kinetics with respect to [Cr(VI)]. However, the zeroth order rate constants decreased with increasing initial chromate concentration, and hysteretic removal rates were observed.

The disparate findings on the reaction order of chromate removal with respect to [Cr(VI)] indicate that the mechanisms involved in chromate removal by iron media are complex, and may not be readily amenable to simple kinetic modeling. This research investigated the mechanisms controlling Cr(VI) removal kinetics, and the factors that control the long-term performance of iron media for chromate removal. A mechanistic understanding of the removal kinetics of Cr(VI) by iron media is essential for designing remedial systems, and for assessing their long-term effectiveness. Tafel analysis and electrochemical impedance spectroscopy (EIS) were used to investigate the reactions that occur on iron media in chromate solutions for three initial iron surface conditions.

3.2.1 Background

The rates of cathodic and anodic reactions occurring on corroding iron can be described by a form of the Butler-Volmer equation as (*62*):

$$i = i_{corr}\left[e^{-\beta_c(E-E_{corr})} - e^{\beta_a(E-E_{corr})}\right] \quad (1)$$

where i is the net current, i_{corr} is the corrosion current, E is iron potential, E_{corr} is the free corrosion potential, and β_c and β_a are the cathodic and anodic Tafel slopes, respectively. In the absence of mass transfer limitations, the β_c and β_a values are indicative of the specific cathodic and anodic reactions that are occurring on the iron surface. Mass transfer limitations of species involved in the cathodic or anodic reactions may lower the observed β_c or β_a values. The first term on the right hand side of equation 1 is proportional to the cathodic current, while the second term is proportional to the anodic current. For an iron potential equal to E_{corr}, the rates of the cathodic and anodic reactions are equal, and the net current (i) is equal to zero. At a potential of E_{corr}, the iron corrodes with a current equal to i_{corr}, the value of which depends on the iron surface area and the concentrations of electroactive species in contact with the iron.

Tafel analysis is based on perturbing the iron potential from E_{corr} by scanning a range in potentials of ±200 mV with respect to E_{corr} (*62*). As indicated by equation 1, decreasing E below E_{corr} increases the rate of the cathodic reactions and decreases the rate of the anodic reactions. At potentials more than ~50 mV below the equilibrium potential for a given redox couple (such as H^+/H_2 or Cr(VI)/Cr(III)) equation 1 predicts a linear relationship between log(i) and the applied potential (E). The slope of this relationship is known as the cathodic Tafel slope (β_c).

In addition to Tafel analysis, EIS is commonly used to study the electrochemical reactions that occur on the surface of corroding iron (*63*). Rates of charge transfer reactions may be controlled by slow rates of electron transfer, slow rates of preceding

chemical reactions, or by diffusional mass transfer limitations. In terms of their effect on the flow of electrons, these three mechanisms can be considered analogous to resistance, capacitance and inductance, respectively, in an alternating current (AC) circuit. This analogy allows the effect of these three mechanisms on the observed reaction rates to be assessed using EIS (*63, 64*).

EIS techniques measure the phase shift between a sinusoidally varying applied potential and the resulting current over a wide range in frequency. Corroding metals are often modeled with the Randles equivalent circuit, as illustrated in Figure 1 (*64*). The impedance (Z) is the resistance to the flow of alternating current, and depends on the solution resistance (R_s), the frequency of the AC signal (ω), the capacitance of the electrical double layer and/or oxides coating the iron surface (C), and the overall charge transfer resistance (R_{ct}). Rates of the electron transfer step are controlled by R_{ct}, which depends on the kinetic facility of both the cathodic and anodic reactions. Because the cathodic and anodic reactions occur in series, the R_{ct} is the sum of the anodic (R_{ct}^a) and cathodic (R_{ct}^c) charge transfer resistances, as given by:

$$R_{ct} = R_{ct}^c + R_{ct}^a \tag{2}$$

The anodic reactions in this study involved iron oxidation to Fe^{2+}, while the cathodic reactions involved water or Cr(VI) reduction. Because water and chromate compete for cathodic sites and their reductions occur in parallel, the R_{ct}^c can be expressed in terms of the charge transfer resistances for water (R_{ct}^w) and chromate (R_{ct}^{Cr}) reduction as:

$$\frac{1}{R_{ct}^c} = \frac{\theta}{R_{ct}^{Cr}} + \frac{1-\theta}{R_{ct}^w} \tag{3}$$

where θ is the fraction of the cathodic sites that are involved in Cr(VI) reduction.

The overall charge transfer resistance may be dominated by either the anodic or cathodic reactions (*65*). Under anodically controlled conditions, the rate at which oxidants are able to accept electrons is faster than the rate at which the iron is able to release electrons. In contrast, cathodically controlled corrosion occurs when the rate at which oxidants are able to accept electrons is slower than the rate at which the iron is able to release electrons. The condition of the iron surfaces, mass transfer effects, and the charge transfer resistances of the pertinent electroactive species determine whether iron corrosion is anodically or cathodically controlled.

3.3 Materials and Methods

Experiments measuring Cr(VI) removal rates were performed in 240 mL sealed plastic cells using three 9 cm long iron wires, or in 850 mL sealed glass cells using one 10 cm long wire. The 1.2 mm in diameter iron wires were of 99.9% purity (Sigma, St. Louis, MO), and were suspended vertically through ports in the lid of the reaction cells. Tafel and EIS analyses were performed in a 15 mL glass electrochemical cell containing a 3.2 cm long wire as the working electrode, a $Hg/HgSO_4$ reference electrode, and a platinum wire counter electrode. All experiments were conducted in solutions that were purged with humidified nitrogen gas in order to agitate the solutions and maintain anaerobic conditions.

Chromate solutions were prepared by adding Na_2CrO_4 to 3 mM $CaSO_4$ background electrolyte solutions. All experiments were performed with initial Cr(VI) concentrations

of 10,000 μg/L. No pH adjustments or buffers were used, and pH values were determined using pH test paper. Throughout the course of the experiments, pH values remained within ±1 pH unit of neutral pH. Aqueous Cr(VI) concentrations were determined using a Dionex (Sunnyvale, CA) model DX500 ion chromatograph with a minimum detection limit of 20 μg/L.

Because Cr(VI) reaction rates in prior investigations have been observed to be hysteretic (*553*, *61*), experiments were performed for three initial surface conditions of the iron wires. Experiments were performed on initially oxide-free iron wires after cathodically polarizing the wires at -2000 mV with respect to the standard hydrogen electrode for five minutes in the background electrolyte solutions. This procedure has been shown to reduce surface oxides to zerovalent iron (*66*, *67*). Experiments with iron coated with a water-formed oxide were conducted by first contacting the iron wire with the background electrolyte solution for 6 days prior to Cr(VI) addition. Experiments were also performed on iron wires coated with an air-formed oxide. These wires underwent no treatment prior to their immersion in the chromate solutions.

3.3.1 Electrochemical Analyses

Tafel analyses were performed to assess the effect of chromate on the cathodic and anodic reactions. All Tafel diagrams were produced by polarizing the wires ±200 mV with respect to their open circuit potentials (*62*). The polarization experiments were performed using an EG&G (Oak Ridge, TN) model 273A scanning potentiostat and M270 software. All potentials are reported with respect to the standard hydrogen electrode (SHE).

The EIS experiments were performed using an EG&G model 273A potentiostat coupled with an EG&G model 5210 impedance phase analyzer. The impedance measurements were performed by applying a sinusoidal waveform with an amplitude of ±10 mV over a frequency range from 5×10^{-3} to 10^{4} Hz. The impedance data were fitted using EG&G ZsimpWin software to a modified Randles circuit where the capacitor was replaced by a constant phase element in order to account for surface roughness and heterogeneities (*68*, *69*). The fit of the experimental data to the modified Randles circuit was very good with chi square values ranging from 0.005 to 0.5.

3.4 Results and Discussion

Figure 2 compares chromate removal rates by iron wires with air and water-formed oxides in two 240 mL reactors. The iron wire with the water-formed oxide exhibited Cr(VI) removal kinetics that were zeroth order with respect to the aqueous Cr(VI) concentration. The removal kinetics by the wire with the air-formed oxide cannot be described by a simple kinetic model. Faster removal kinetics were observed on the first day elapsed than on subsequent days, where the removal rates could be described by a zero order kinetic model. A similar finding of a fast initial uptake followed by slower long-term rates has been attributed to a fast adsorption mechanism accompanying a slower reaction mechanism (*58*). Based on Cr(VI) removal rates after the first day elapsed, the zero order rate constant (k_o) for the wire with the air-formed oxide of 1.2±0.4 $\mu g/cm^2$/day was a factor of 8 smaller than that for the wire with the water-formed oxide, which had a k_o 10±1.3 $\mu g/cm^2$/day. Similar behavior was observed in the 850 mL

reactors where there was also an initial rapid uptake by the wire with the air-formed oxide, followed by zero order removal kinetics until the experiment was terminated after 80 days elapsed. The k_o values in the 850 mL reactors were statistically identical to those in the 240 mL reactors, and were 12.1±3.7 and 1.1±0.2 $\mu g/cm^2/day$ for the water and air-formed oxides, respectively. The removal kinetics exhibited in Figure 2 show that short-term batch tests lasting less than one day using iron coated with air-formed oxides may not be useful for determining steady state Cr(VI) removal rates.

Although the rate constants for Cr(VI) removal differed by an order of magnitude between the two types of wires, Figure 2b shows that the corrosion rates of the two wires were similar. This indicates that the corrosion rate is not a good indicator of the effectiveness of iron media for Cr(VI) removal. To elucidate the mechanisms responsible for the removal rate and corrosion behavior exhibited in Figure 2, Tafel and EIS analyses were used to investigate the effect of surface oxides on the reactions occurring on iron media in chromate solutions.

Figure 3 shows Tafel and EIS plots for an initially oxide free iron wire after addition of 10,000 μg/L Cr(VI) to the $CaSO_4$ electrolyte solution. As shown in Figure 2b, addition of Cr(VI) to the blank solution resulted in an approximately 10% decrease in the corrosion current by 30 minutes elapsed. This decrease in i_{corr} was accompanied by an approximately 100 mV increase in the free corrosion potential, as shown in Figure 2c. The decrease in corrosion rate at 30 minutes can be primarily attributed to a decrease in the rate of water reduction due to the 100 mV increase in E_{corr}. According to the β_c value of 0.0052 dec/mV determined in the blank solution, a 100 mV increase in E_{corr} should be

associated with a factor of 3.3 decrease in the current for water reduction. The smaller than anticipated decline in current at 30 minutes indicates that there was direct reduction of Cr(VI) at the iron surface at early elapsed times. The increase in cathodic current at all potentials in the Tafel scan, and the change in β_c accompanying chromate addition, are also indicative of a change in the cathodic reaction from that of water reduction only, to the combined reactions of water and Cr(VI) reduction.

Other evidence for direct Cr(VI) reduction at early elapsed times can be seen in the EIS profiles in Figure 3b. Upon addition of Cr(VI) to the blank solution, the R_{ct} dropped from 11,800 to 8200 Ω. However, at all potentials the anodic currents were lower in the Cr(VI) solutions, indicating an increase in R_{ct}^{a}. Therefore, the drop in R_{ct} shows that the overall rate of corrosion was cathodically controlled in both the blank, and in the Cr(VI) solution before 1 day elapsed. In this case, the rate of iron corrosion was limited by the rate at which oxidants were able to accept electrons, and not by the rate at which the iron was capable of releasing electrons. The 30 minute EIS profile and equation 3 also show that the R_{ct}^{Cr} was smaller than R_{ct}^{w}.

Between 1 and 5 days elapsed, the cathodic currents continued to decrease as Cr(VI) was removed from solution. This was confirmed by measurement of the aqueous Cr(VI) concentration which showed that 97% of the chromate had been removed by 5 days elapsed. This amount of removal over 5 days corresponds to a k_o of 24 $\mu g/cm^2$/day. The permanent increase in the cathodic currents over that in the blank can be attributed to the presence of oxides on the iron surface that increased the cathodic area for water reduction.

In contrast to the greater cathodic currents after addition of Cr(VI) to the solution, there was a permanent decrease in anodic currents after Cr(VI) addition. This decrease can be attributed to a permanent increase in the R_{ct}^{a}. In contrast, the higher currents in the cathodic profiles show that the R_{ct}^{c} after five days elapsed was less than that in the blank solution. Thus, according to equation 2, the overall increase in R_{ct} that occurred between 1 and 5 days elapsed, and the decreasing corrosion currents, must be attributed to an increase in R_{ct}^{a} associated with chromium and iron oxides blocking anodic sites on the iron surface.

Tafel and EIS profiles for an iron wire that was equilibrated with the blank electrolyte solution for 6 days prior to Cr(VI) addition are shown in Figure 4. Over the first 6 days elapsed in the blank electrolyte solution there was a slight increase in cathodic currents and a decrease in R_{ct}. This can be attributed to reduction of the air-formed oxide, and an increase in surface area that decreased the R_{ct} from 10,900 to 8,300 Ω between 1 and 6 days. Upon addition of Cr(VI) to the solution, the E_{corr} value increased by 50 mV, as shown in Figure 2c. According to the β_c value of 0.0064 dec/mV in the blank at 6 days, this increase in potential should have resulted in a factor of 2 decline in the current for water reduction. However, as shown in Figure 1b, there was only a 25% decline in i_{corr} upon Cr(VI) addition. Since the overall corrosion rate was cathodically controlled in the blank solution, the smaller than anticipated decline in i_{corr} shows that Cr(VI) directly oxidized the iron at early elapsed times. Similar to the oxide free case, Cr(VI) addition resulted in increased cathodic currents and decreased anodic currents compared to those in the blank electrolyte. However, in contrast to the decrease in R_{ct} that was observed

upon Cr(VI) addition in the oxide-free case, the R_{ct} increased from 8,300 to 13,300 Ω after Cr(VI) addition. This shows that the decrease in R_{ct}^{c} due to Cr(VI) was more than compensated by an increase in R_{ct}^{a}.

Between days 4 and 7 elapsed after Cr(VI) addition, the anodic currents increased by more than a factor of 5 while the cathodic currents decreased by less than a factor of 2. The declining cathodic currents are similar to those for the oxide-free case, and can be attributed to a declining contribution of Cr(VI) reduction to the overall corrosion rate. The increasing anodic currents after 4 days elapsed are contradictory to the oxide-free case of declining anodic currents, and were accompanied by an overall decrease in R_{ct} from 15,500 to 9800 Ω. The decreasing cathodic currents, increasing anodic currents, and the overall decrease in R_{ct} show that the overall rate of iron corrosion was anodically controlled between 4 and 7 days. Under this condition, rates of the cathodic reactions of water and Cr(VI) reduction were limited by the rate at which the iron could release Fe^{2+} at anodic sites, and not by their own intrinsic reaction rates.

The recovery in anodic currents shown in Figure 4a that occurred only after 4 days elapsed shows that Cr(VI) concentrations as low as 2500 μg/L are capable enforcing anodically passivating oxides. Based on the complete Cr(VI) removal that was observed after 7 days, ~57% of the chromate had been removed by the fourth day elapsed. However, there was only a small recovery in the anodic current by that time. However, once ~75% the Cr(VI) was removed by the fifth day, there was a rapid decline in the degree of anodic passivation, as indicated by drops in E_{corr} (Figure 2c) and R_{ct} between 4 and 5 days. By seven days elapsed, Figure 2b shows that the corrosion current had

reached close to its value before the addition of chromate.

Figure 5a shows Tafel profiles for an iron wire with an air-formed oxide after placement in a 10,000 μg/L Cr(VI) solution. As indicated by the corrosion currents in Figure 2b, the i_{corr} at 30 minutes elapsed for the iron with the air-formed oxide was approximately 75% of that for the oxide-free iron. However, the E_{corr} was more than 100 mV greater than that for the oxide-free case. The higher potential can be attributed to the preservation and reinforcement of the oxide film due to the oxidizing ability of chromate. In contrast to the cases of the oxide-free and water-formed oxide surfaces, chromium can repair and reinforce cracks and structural defects in the air-formed oxide resulting in a uniform protective film (*70*). The reinforced air-formed oxide film is associated with high R_{ct}^{a} values that result from restricted diffusion of Fe^{2+} away from anodic sites. The high R_{ct}^{a} resulted in R_{ct} values that were 5 to 8 times greater than those for the oxide-free and water-formed oxide wires.

The decreasing anodic and cathodic currents between 30 minutes and 1 day elapsed can be attributed to increasing passivation arising from oxidation of remaining Fe(II) in the air-formed oxide. During the first day elapsed the i_{corr} decreased by 60%, as shown in Figure 2b. After the first day the i_{corr} was stable until increasing by 35% between days 3 and 4. This increase in i_{corr} was associated with the formation of a secondary oxide phase, as indicated by the appearance of a second peak in the Bode phase diagram in Figure 5b. Previous observations of similar phenomena in carbon steel studies revealed the presence of an intermediate, porous, and conductive oxide between the zerovalent iron and the outer Fe(III) oxide layer (*71*). The increase in phase shift due to secondary

oxide formation is consistent with increasing capacitive properties of the oxide. Thus, the secondary oxide appears to mediate the electron transfer from the zerovalent surface to oxidizing species. Formation of the secondary oxide phase was also associated with a decrease in R_{ct} from 115,000 to 70,000 Ω between 3 and 7 days elapsed. The decreasing cathodic currents and increasing anodic currents accompanying the overall decrease in R_{ct} shows that the overall rate of iron corrosion, and thus Cr(VI) reduction, was anodically controlled during this time.

Figure 6 shows Tafel profiles for iron wires with different initial surface conditions approximately 1 week after their immersion in the 10,000 µg/L Cr(VI) solutions. Also shown is a profile for an iron wire immersed in the blank electrolyte after 6 days elapsed. For the water-formed and initially oxide-free wires, the cathodic currents at potentials near the E_{corr} for each wire were the same as those for the blank. This shows that there was no permanent effect of Cr(VI) on the cathodic reactions and cathodic sites after all the Cr(VI) had been removed from the solutions. The cathodic Tafel slopes for the blank, oxide-free, and water-formed oxide cases of β_c=0.006 to 0.0068 dec/mV are indicative of water reduction (*61*, 66, *72*, *73*). The lower cathodic slope for the air-formed oxide can likely be attributed to reduction of Cr(VI), iron oxides, and water. The lower cathodic currents for the air-formed oxide wire at potentials below -550 mV show that there was permanent cathodic passivation.

The anodic profiles in Figure 6 show that there was permanent anodic passivation on all three wires after exposure to chromate. The wire with the water-formed oxide showed the least passivation, most likely attributable to protection of the iron from Cr(VI) by the

oxide film. The high degree of anodic passivation for the wire with the air-formed oxide can be attributed to the ability of Cr(VI) to enforce the air-formed oxide and create a continuous protective film.

The Tafel and EIS analyses showed that in the absence of an air-formed oxide, Cr(VI) was able to directly oxidize the iron, at least at early elapsed times. The Faradaic current efficiency for Cr(VI) reduction can be determined by integrating the corrosion currents in Figure 2b. Assuming three moles of electrons were associated with each mole of Cr(VI) removed, the Faradaic current efficiency for Cr(VI) reduction ranges from 12% for the iron with the air-formed oxide, to 60% for the oxide-free iron. If the reducing capacity of the Fe^{2+} that was released at anodic sites is considered, the Faradaic current efficiency for the air-formed oxide decreases to 8%, while that for the oxide-free case decreases to 40%. The low current efficiency associated with the air-formed oxide suggests that water is much more facile at penetrating the outer Fe(III) oxide to reach cathodic sites. The high current efficiencies in absence of an air-formed oxide show that chromate was able to garner a substantial fraction of the corrosion current at cathodic sites. However, the cathodic Tafel slopes after 1 day elapsed were more indicative of water reduction than that for chromate reduction, which has a β_c value that is more than 3 times greater than that for water reduction. These two facts suggest that in addition to direct electron transfer, chromate may also be indirectly reduced by atomic hydrogen produced from water reduction.

Although chromate was capable of directly oxidizing the iron, the corrosion currents were not proportional to the aqueous Cr(VI) concentrations. This can be attributed to

competition between chromate and water for cathodic sites on the iron surface, and to the anodic control of iron corrosion for chromate concentrations above 2500 μg/L. Because of anodic control, rates of the cathodic reactions were not proportional to the concentration of oxidants in the solution, but were limited by the iron's ability to release Fe^{2+} at anodic sites. This mechanism is consistent with Cr(VI) reduction rates that are zero order in chromate concentration.

3.5 Acknowledgement

This project was made possible by grant number 2P42ES04940-11 from the National Institutes for Environmental Health Sciences of the National Institutes for Health, with funds from the U.S. Environmental Protection Agency.

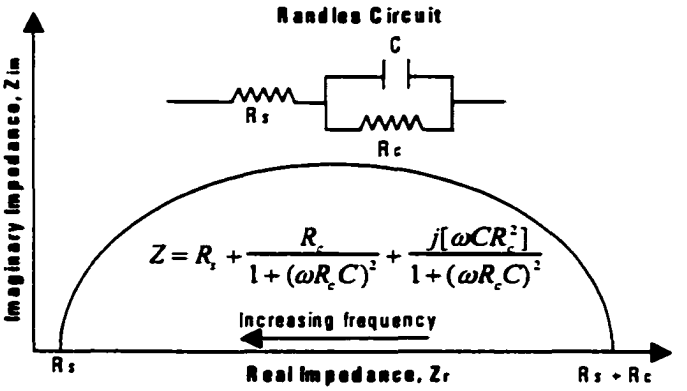

Figure 3.1 Randle's circuit and the corresponding Nyquist plot of real versus imaginary impedance.

Figure 3.2 a. Chromate removal versus time for an iron surface covered with an oxide formed by initial exposure to chromium-free water for 6 days (WFO), and for an iron surface covered with an air-formed oxide (AFO). The zero order constant (k_o) for the air-formed oxide represents the removal after the fast initial removal (dotted line) for the first day elapsed. b. Corrosion rates versus time for iron surfaces with different exposure histories. c. Corrosion potentials corresponding to the corrosion currents shown in Figure 2b.

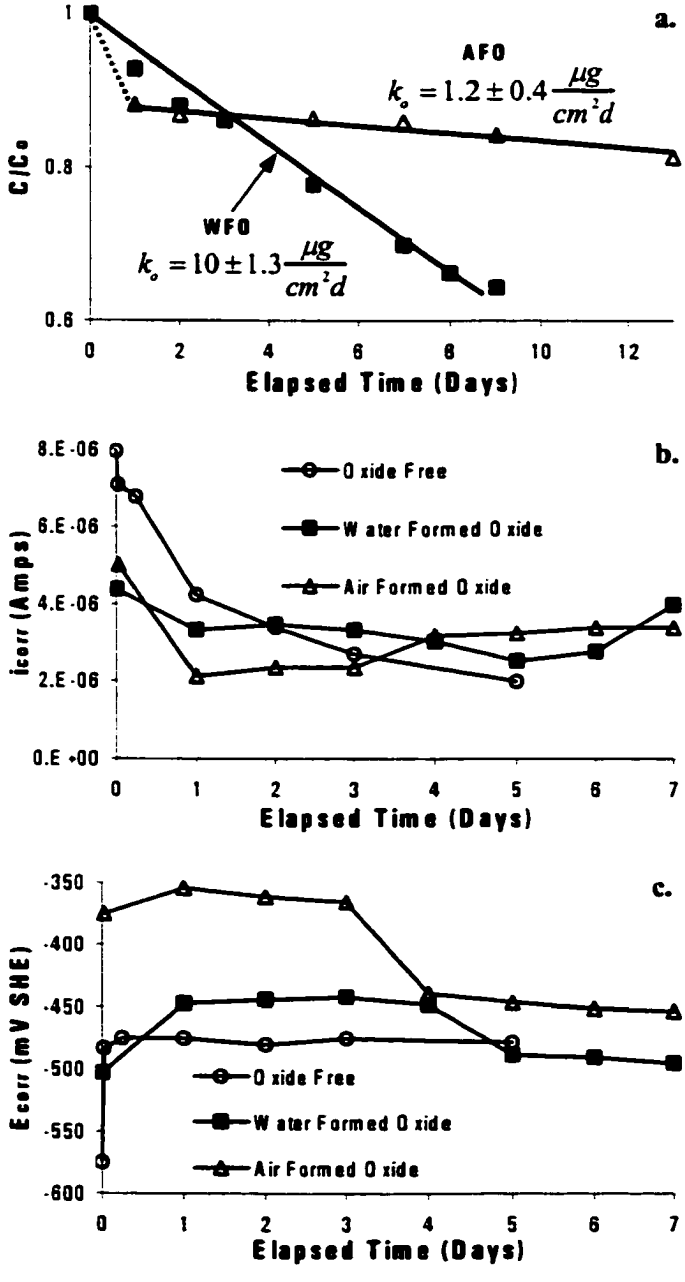
a.
AFO
$k_o = 1.2 \pm 0.4 \frac{\mu g}{cm^2 d}$
WFO
$k_o = 10 \pm 1.3 \frac{\mu g}{cm^2 d}$
C/Co
1
0.8
0.6
0
2
4
6
8
10
12
Elapsed Time (Days)
b.
Oxide Free
Water Formed Oxide
Air Formed Oxide
icorr (Amps)
8.E-06
6.E-06
4.E-06
2.E-06
0.E+00
0
1
2
3
4
5
6
7
Elapsed Time (Days)
c.
Ecorr (mV SHE)
-350
-400
-450
-500
-550
-600
Oxide Free
Water Formed Oxide
Air Formed Oxide
0
1
2
3
4
5
6
7
Elapsed Time (Days)

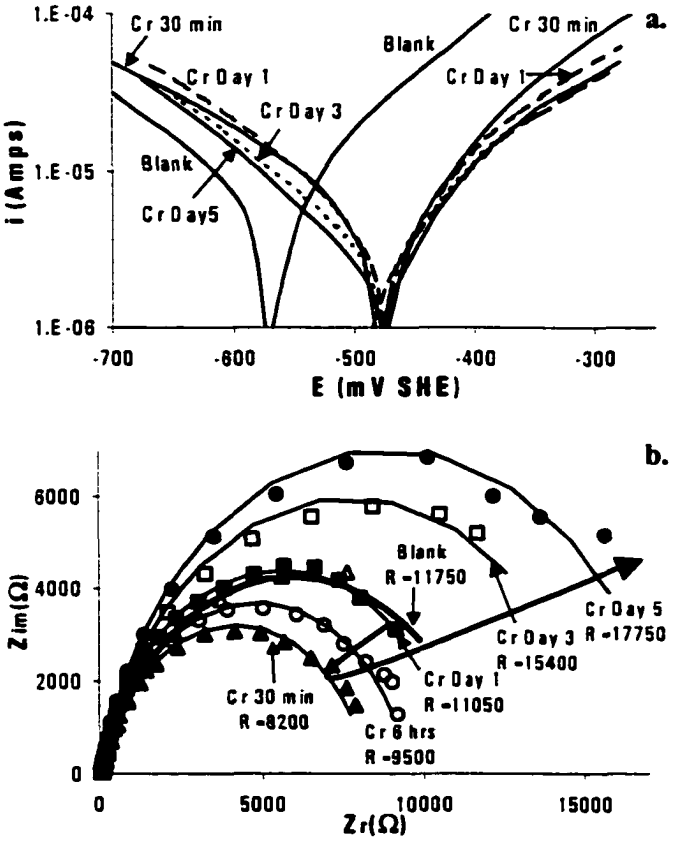

Figure 3.3 a. Tafel diagrams at different elapsed times for an initially oxide-free iron surface. b. Nyquist plots at different elapsed times for the oxide-free surface. The surface was cathodically polarized to remove oxides. Blank measurements were taken prior to chromate addition.

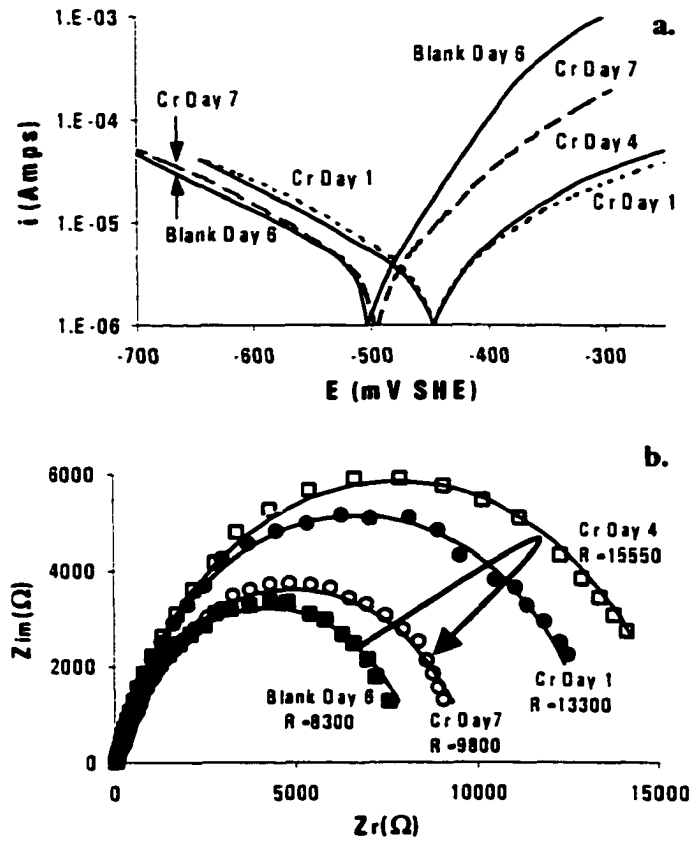

Figure 3.4 a. Tafel diagrams for an iron surface covered with a water-formed oxide. b. Nyquist plots at different elapsed times for an iron surface surface covered with a water-formed oxide. The iron surface was exposed to chromium-free water for 6 days prior to chromate addition. The blank shown is for 6 days elapsed in the chromium-free solution.

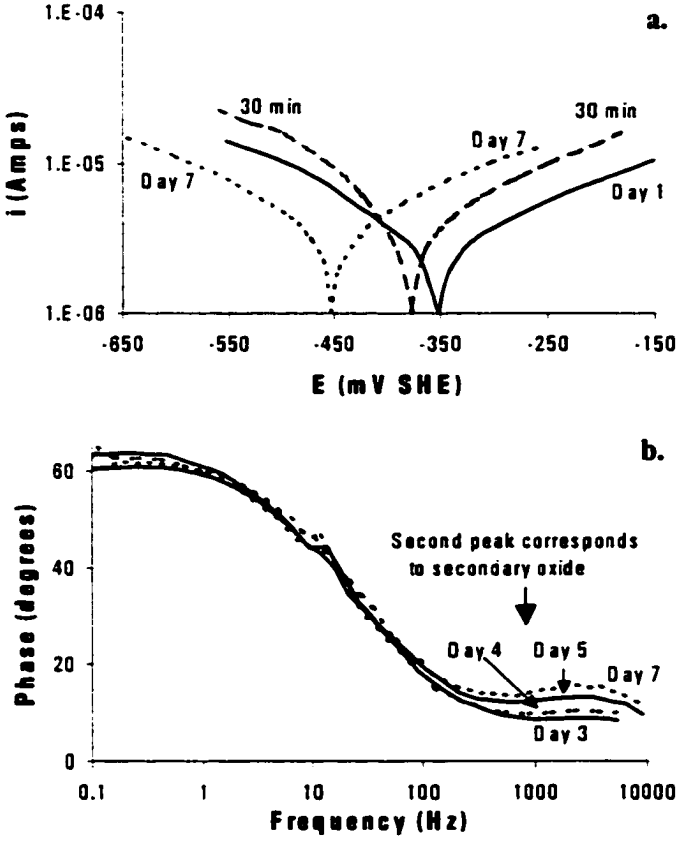

Figure 3.5 a. Tafel diagrams for an iron surface with an air-formed oxide. b. Bode phase plots for the iron surface with an air-formed oxide.

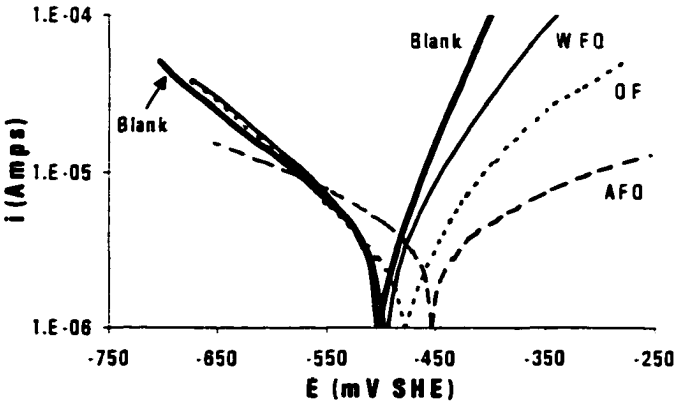

Figure 3.6 Tafel diagrams produced at the termination of each experiment for a water-formed oxide (WFO), an air-formed oxide (AFO) and an oxide-free (OF) initial condition. The blank diagram corresponds to the surface exposed at chromium-free water for 6 days.

CHAPTER 4

UNDERSTANDING SOLUBLE ARSENATE REMOVAL KINETICS BY ZEROVALENT IRON MEDIA

4.1 Abstract

Zerovalent iron filings have been proposed as a filter medium for removing arsenic compounds from potable water supplies. This research investigated the kinetics of arsenate removal from aqueous solutions by zerovalent iron media. Batch experiments were performed to determine the effect of the iron corrosion rate on the rate of As(V) removal. Tafel analyses were used to determine the effect of the As(V) concentration on the rate of iron corrosion in anaerobic solutions. As(V) removal in column reactors packed with iron filings was measured over a one-year period of continuous operation. Comparison of As(V) removal by freely corroding and cathodically protected iron showed that rates of arsenate removal were dependent on the continuous generation of iron oxide adsorption sites. In addition to adsorption site availability, rates of arsenate removal were also limited by mass transfer associated with As(V) diffusion through iron corrosion products. Steady state removal rates in the column reactor were up to 10 times faster between the inlet-end and the first sampling port, than between the first sampling port and the effluent-end of the column. Faster removal near the influent-end of the column was due to a faster rate of iron oxidation in that region. The presence of 100 μg/L As(V) decreased the iron corrosion rate by up to a factor of five compared to a blank electrolyte solution. However, increasing the As(V) concentration from 100 to 20,000 μg/L resulted in no further decrease in the iron corrosion rate. The kinetics of

arsenate removal ranged between zeroth and first-order with respect to the aqueous As(V) concentration. The apparent reaction order was dependent on the availability of adsorption sites and on the aqueous As(V) concentration. X-ray absorption spectroscopy analyses showed the presence of iron metal, magnetite (Fe_3O_4), a Fe(III) oxide phase, and possibly a Fe(II,III) hydroxide phase in the reacted iron filings. These mixed valent oxide phases are not passivating and permit sustained iron corrosion and continuous generation of new sites for As(V) adsorption.

4.2 Introduction

The concern over arsenic in drinking water has increased in recent years due to the discovery of high levels of arsenic in potable water supplies in several developing nations (*74, 75*). In the United States, the Environmental Protection Agency has recently decreased the maximum contaminant level (MCL) for arsenic in drinking water from 50 to 10 μg/L (*76*). The heightened awareness of arsenic toxicity and the proposed regulatory changes have prompted considerable research efforts towards developing new methods for removing arsenic from drinking water.

Several investigators have proposed the use of zerovalent iron filings as a filter medium for removing As(V) (arsenate) and As(III) (arsenite) compounds from drinking water (*77-82*). The operational simplicity of zerovalent iron filters make them suitable for point of use, individual well-head, or other small-scale treatment systems. Some investigators (*82*) have reported that As(V) species may be reduced by zerovalent iron to As(III), but others have reported no reduction of As(V), even after more than 1 year of

contact time (*80, 81*). Reduction notwithstanding, the removal mechanism for both As(III) and As(V) compounds involves adsorption to iron oxides (*77, 80-82*). Some investigators have reported more favorable adsorption of As(III) versus As(V), while others have reported more favorable adsorption of As(V) (*80, 82*). Differences in the relative ease of As(V) versus As(III) removal can likely be attributed to differences in iron oxide morphology, iron oxidation state, water chemistry, and pH between investigations (*77*).

Adsorption and coprecipitation of arsenite and arsenate on Fe(III) oxides have been thoroughly investigated (*83-92*). The removal mechanisms involve both mono- and bi-dentate complex formation with ferric oxyhydroxides (*86, 87, 91*). Grossl *et al.* (*87*) showed that arsenate uptake by goethite initially occurs via a ligand exchange mechanism that replaces a surface bonded OH^- (>Fe-OH) by a monodentate arsenate ion. The monodentate complex may then transform into an inner-sphere bidentate complex. X-ray absorption spectroscopy (XAS) studies indicate the predominance of bidentate arsenate surface complexes over monodentate, but that may be a function of the As(V) concentration, pH, equilibration time, and the properties of the iron oxide phase (*86, 91, 93-95*).

Reactions of arsenic compounds with Fe(II) have received much less attention than those involving Fe(III). This is likely due to the instability of ferrous oxides in water, which convert to magnetite or one of many possible ferric oxide phases over time periods of hours to days (*96*). However, one study investigating the effect of Fe^{2+} and Fe^{3+} ions on arsenate removal by activated carbon showed that Fe^{2+} was more effective in

promoting arsenate removal (*97*). Enhanced removal of arsenate by Fe^{2+} was attributed to precipitate formation, since the adsorption process appeared to be irreversible.

The kinetics of arsenate removal by a range of ferric oxides has been investigated in several studies (*84, 85, 87, 88*). Grossl et al. (*87*) used a pressure jump/relaxation technique to investigate the kinetics of arsenate surface complex formation with goethite. That study found that formation of monodentate ferric-arsenate complexes occurred on a time scale of milliseconds, while transformation to bidentate complexes occurred on a time scale of seconds. Given the rapidity of surface complex formation, the slow approach to sorptive equilibrium (often requiring hours or days to reach) has been attributed to the slow diffusion of arsenic species through porous iron oxides (*85*). Aging of amorphous iron oxides to more stable phases with different arsenate sorption capacities may also contribute to the slow approach to sorptive equilibrium.

The kinetics of arsenic removal by zerovalent iron media has been the subject of several recent investigations. Lackovic *et al.* (*80*) reported on the removal kinetics of As(III) and As (V) in terms of removal efficiencies. This type of kinetic information is case specific, and is therefore not useful for extrapolation to other experimental conditions. Su and Puls (*82*) used a first-order model to describe As(III) and As(V) removal kinetics in short-term batch tests lasting less than 4 days. In that study, the capacity of iron for arsenic removal was described using a Langmuir adsorption model. However, because iron is reactive and continuously generates new adsorption sites via corrosion, short-term batch tests conducted at high concentrations may not be useful for

assessing iron's long-term performance for removing arsenic from low concentration solutions.

In a recent study, Farrell *et al.* (*81*) showed that arsenate removal kinetics by corroding iron in batch tests could be described by a kinetic model of the form:

$$\frac{d[As]}{dt} = \frac{-k_0[As]}{k_0/k_1 + [As]} \quad (1)$$

where [As] is the arsenate solution concentration, t is time, k_0 is the zeroth-order rate constant, and k_1 is the first-order rate constant. This form of kinetic expression yields removal rates that approach first-order in [As] in the limit of infinite dilution, and zeroth order in [As] at infinite concentration. First-order removal kinetics occur when there is an excess of adsorption sites, and thus, there is no sorptive competition among dissolved As(V) species for these sites. In this case, arsenate removal rates are limited by the rate of mass transport to adsorption sites within the porous oxides.

At early elapsed times after an oxide-coated zerovalent iron sample is placed into an arsenate solution, approximately pseudo-first-order kinetics may be observed due to mass transfer limitations. However, with increasing elapsed time, deviation from pseudo-first-order kinetics will occur if the rate of Fe^{2+} generation is less than the rate of arsenate removal. This arises from competition between arsenate species for a decreasing number of adsorption sites. For a fixed rate of iron corrosion, competition for adsorption sites increases with increasing As(V) concentration. At high As(V) concentrations, the removal kinetics approach pseudo-zeroth order, and are limited by the rate of adsorption site generation.

The purpose of this investigation was to assess the validity of the kinetic model in equation 1 for describing the long-term removal of arsenate by packed beds of zerovalent iron filings. Batch experiments were performed to assess the effect of the iron corrosion rate on the rate of arsenate removal, and to assess the effect of the arsenate concentration on the rate of iron corrosion. Column experiments were performed to determine long-term arsenate removal rates by packed beds of iron filings as a function of the influent arsenate concentration. X-ray absorption spectroscopic analyses were performed to determine the identity of iron corrosion products and their relationship to arsenate removal rates.

4.3 Materials and Methods

4.3.1 Batch Reactors

Two batch experiments were performed to determine the influence of the iron corrosion rate on rate of the arsenate removal. Arsenate removal by freely corroding and cathodically protected iron wires was measured in 3 mM $CaSO_4$ background electrolyte solutions containing Na_2HAsO_4 at an initial As(V) concentration of 100 µg/L. Cathodic protection in one of the reactors was accomplished by polarizing the iron by -100 mV with respect to its free corrosion potential. Each glass batch reactor contained 850 mL of solution at pH 7, a 10 cm long by 1.2 mm diameter iron wire of 99.9% purity (Aesar, Ward Hill, MA), a calomel reference electrode (EG&G, Oak Ridge, TN), and a stainless steel wire counter electrode. A platinum wire electrode that was intermittently inserted through the sampling port on each reactor was used to measure the solution redox potential. The reactors were purged with 50 mL/min of humidified nitrogen gas in order

to agitate the solutions and maintain anaerobic conditions. The solution potentials of –390 to -425 mV, with respect to the standard hydrogen electrode (SHE), confirmed that dissolved oxygen concentrations in both reactors were low.

A batch experiment was also performed to measure arsenate removal by a freely corroding iron wire under steady state conditions. In this experiment a 117 μg/L solution of As(V) in a 3 mM $CaSO_4$ electrolyte was pumped through a 250 mL stirred, batch reactor at a flow rate of 1 mL/min. Iron corrosion rates and effluent arsenate concentrations were then periodically measured.

A fourth batch experiment was performed to determine the effect of arsenate concentration on the iron corrosion rate. In this experiment, a single 10 cm long iron wire was placed in a nitrogen-purged, 3 mM $CaSO_4$ electrolyte solution. The corrosion rate of the iron in the blank solution was then measured over a ten-day period until it reached a steady state. On subsequent days, arsenate was added to the reactor through the sampling port to achieve As(V) concentrations ranging from 100 to 20,000 μg/L. The corrosion rate of the iron was then measured after one day elapsed at each arsenate concentration.

4.3.2Column Experiments

Column experiments were performed using either a 50 cm long by 2.5 cm outer diameter (o.d.) glass column, or a 25 cm long by 0.9 cm o.d. stainless steel column. Both columns were packed with Master Builder's Supply (Cleveland, OH) iron filings GX-27 blend. The iron filings were coated with an air-formed oxide and were used as received. The glass column contained an inlet and three intracolumn sampling ports at 0, 12.5, 25, and

37.5 cm from the influent end. One port at each location served for taking aqueous samples and for measuring the redox potential of the solution. The other port was used to determine how the iron corrosion rate and free corrosion potential varied along the length of the column. The corrosion rates and potentials were measured using an iron wire permanently inserted into the column through a rubber septum at each port. A stainless steel screen placed above each sampling port was used to prevent the filings in the column from contacting the iron wire probes. The columns were operated with As(V) concentrations ranging from 100 to 50,000 μg/L in nitrogen-purged, 3 mM $CaSO_4$ background electrolyte solutions. The glass column was operated with mean hydraulic residence time of 20 minutes, and was operated at each influent concentration until a steady state effluent concentration was attained. The stainless steel column was operated with hydraulic residence times of 20 seconds or 25 minutes, but in several instances the influent concentrations were changed before reaching steady state arsenic removal.

4.3.3 Analytical Methods

Total arsenic and iron concentrations in the aqueous phase were determined with a graphite furnace atomic absorption (AA) spectrophotometer (Perkin Elmer, San Jose, CA) using a published method (*98*). The oxidation state of aqueous arsenic species was determined via ion chromatography (IC) using an atomic fluorescence detector (PS Analytical, Kent, UK). The detection limits for the AA and IC methods (*99*) were both ~1 μg/L. Corrosion currents (I_{corr}) and free corrosion potentials (E_{corr}) were measured by analysis of Tafel diagrams produced by polarizing the iron wire electrodes ±150 mV with respect to their open circuit potentials (*81, 100*). The polarization experiments were

performed using an EG&G model 273A scanning potentiostat and EG&G M270 software.

4.3.4 X-ray Absorption Spectroscopy

Iron K-edge X-ray absorption spectra for iron filing samples from the influent and effluent ends of the stainless steel column were collected at the Stanford Synchrotron Radiation Laboratory (SSRL) on wiggler beamlines 4-1 and 4-3 under dedicated conditions (3 GeV, 70-90 mA). Spectra for the filings and solid reference compounds were collected in transmission mode at room temperature using Si(220) monochromator crystals and gas-filled ion chambers. All samples were prepared in an anaerobic glove box and placed in airtight containers prior to analysis (*81*). Bulk samples were powdered and mounted as thin, uniform smears on adhesive tape. Beam energy was calibrated by setting the first inflection of an iron foil spectrum to 7112.0 eV. Four scans were collected and averaged for each sample. First-derivative X-ray absorption near-edge structure (XANES) spectra were fit by linear combination with reference compounds using the program DATFIT (*100*) to qualitatively determine the primary iron phase(s). Numerical results were extracted from extended X-ray absorption fine structure (EXAFS) spectra using the computer program EXAFSPAK (*101*), and theoretical phase-shift and amplitude reference functions were calculated using the program FEFF6 (*102*). Numerical values for interatomic distances (R), number of backscatters (N), Debye-waller factor (σ^2) and ΔE_0 (one variable for all atomic shells) were determined by non-linear least-squares fits to background-subtracted, normalized spectra. To reduce the number of independent variables in fits, σ^2 was fixed on typical values determined from

reference compounds (*103*), and interatomic distances (R) for selected atomic shells were fixed on crystallographic values of phases identified in the XANES analyses.

4.4 Results and Discussion

4.4.1 Batch Reactors

The relationship between the arsenate removal rate and the rate of iron oxidation was investigated by comparing arsenate removal rates by freely corroding and cathodically protected iron. Aqueous arsenate concentrations in the batch reactors as a function of elapsed time are shown in Figure 1. In all batch reactors, solution pH values remained constant at 7 ± 0.5. The rate of arsenate removal by the freely corroding iron wire conformed to the kinetic model described by equation 1. Over the first three days, the arsenate removal rates by the cathodically protected iron were similar to those observed with the freely corroding iron. However, after that time the rate of arsenate removal by the cathodically protected iron was significantly slower than that for the freely corroding iron. The As(V) removal rate between 3 and 14 days elapsed for the cathodically protected wire yielded a first-order rate constant (k_1) of 0.010 d^{-1}, which is 10 times smaller than the k_1 for the freely corroding iron of 0.1 d^{-1}.

The similar removal rates during the first three days can be explained by arsenate adsorption to oxides present on the iron wires at the time of their immersion into the As(V) solutions. The slower removal by the cathodically protected iron after 3 days can be attributed to a slower generation rate of new adsorption sites. Cathodic protection decreased the iron oxidation current by two orders of magnitude from 0.2 to 0.002 μA.

The decrease in removal rate with the decrease in anodic current clearly shows that the removal rate was tied to the rate of Fe^{2+} generation. Although the freely corroding anodic current was two orders of magnitude larger than the cathodically protected anodic current, its first-order rate constant was only one order of magnitude larger. The lack of proportionality between the corrosion rate and the removal rate is consistent with greater mass transfer limitations associated with a thicker oxide on the freely corroding iron.

The relationship between the arsenate removal rate and the iron corrosion rate was investigated under steady state removal conditions. Figure 2a shows the effluent arsenate concentrations from the flow-through reactor, and Figure 2b shows the associated corrosion currents. The steady state removal of 40 μg/L As(V) corresponds to a removal rate of 0.78 μmoles per day. This compares to an Fe^{2+} generation rate of 3.6 μmoles/day, based on an average corrosion rate of 8 μA. The factor of 4.6 greater rate of Fe^{2+} generation versus As(V) removal suggests that arsenate removal under steady state conditions was limited by diffusion through the oxide layer to adsorption sites. This conclusion is supported by comparing rates of As(V) removal and iron corrosion in the nitrogen-purged and flow-through reactors. At a concentration of 77 μg/L, the removal rate in the flow-through reactor of 0.78 μmoles/d was a factor of 9 times greater than the removal rate of 0.087 μmoles/d in the nitrogen-purged reactor. However, the corrosion rate in the flow-through reactor was approximately 40 times greater than that in the nitrogen-purged reactor (due to higher dissolved oxygen concentrations). This suggests that there were greater mass transfer limitations associated with the thicker oxide on the faster corroding iron in the flow-through reactor.

The effect of arsenate concentration on the corrosion rate of an iron wire immersed in solutions with concentrations between 0 and 20,000 μg/L is shown in Figure 3. An arsenate concentration of 100 μg/L decreased the iron corrosion rate by a factor of 5 as compared to that in a blank electrolyte solution. However, increasing the arsenate concentration from 100 to 20,000 μg/L had no measurable effect on the corrosion rate. This can be explained by the mechanism through which arsenate affects iron corrosion, as determined in a previous investigation (*81*). Adsorption of arsenate at cathodic sites blocks water reduction, and thereby lowers the iron corrosion rate, becaues arsenate itself is not reduced (*81*). The absence of a concentration dependence in Figure 3 can therefore be attributed to cathodic site saturation at As(V) concentrations as low as 100 μg/L.

4.4.2 Column Reactors

The applicability of the kinetic model in equation 1 to column reactors was investigated for influent arsenate concentrations ranging from 100 to 50,000 μg/L. The influent concentration history for the glass column reactor is summarized in Table 1. In all column reactors, effluent pH values were identical to influent values of 7 ± 0.5. Iron concentrations in the column effluent remained at ~40 μg/L regardless of the influent As(V) concentration. The low dissolved iron concentrations and the constant pH values can be attributed to precipitation of $Fe(OH)_{2(s)}$ on the iron surfaces. All the arsenic adsorbed to the iron particles was in the +5 oxidation state (*81*).

For influent concentrations below 1,000 μg/L, complete arsenate removal was observed before the first sampling port. However, for influent As(V) concentrations of 2,500 μg/L and greater, breakthrough was observed at all sampling ports, as shown by the

data in Figure 4a for influent concentrations between 2,500 and 10,000 μg/L. Arsenate breakthrough at all ports shows that site saturation limited As(V) removal rates for feed concentrations of 2,500 μg/L and greater.

For all feed concentrations, the arsenate removal rate was faster before the first sampling port than between the first port and the effluent end of column. A similar observation of faster removal near the inlet end of several columns packed with iron filings was reported by Lackovic *et al.* (*80*) for both As(V) and As(III) removal. The faster removal near the column inlet can be explained by the corrosion current data in Figure 4b. Throughout the month-long test, the iron corrosion rate at the influent end of the column was at least a factor of seven times greater than the corrosion rate at any of the three intracolumn sampling ports, as illustrated in Figure 4b. The faster corrosion rates near the column inlet were present in both the blank and As(V) containing solutions. Therefore, they cannot be attributed to differences in As(V) concentration between the inlet and the three intracolumn sampling ports.

The faster corrosion rate near the column inlet can be attributed primarily to trace amounts of oxygen in the influent water. Although the influent water reservoir was purged with nitrogen, analysis of Tafel diagrams shows the presence of oxygen at the inlet port. Figure 4c shows representative Tafel diagrams produced at the inlet and middle ports of the column. For the middle sampling port, the cathodic Tafel slope of 0.006 dec/mV was close to slopes of 0.0060 to 0.0072 dec/mV that have been observed for water reduction in several previous investigations (*104-106*). However, the cathodic Tafel slope of 0.003 dec/mV for the inlet sampling port was considerably smaller. This

smaller cathodic slope can most likely be attributed to mass transfer limited oxygen reduction. The presence of oxygen in the influent water is also indicated by the higher redox potential of the influent solution compared to that observed at the intracolumn sampling ports. The nitrogen-purged influent solution had a redox potential range of 300 to 400 mV, while the solution potential within the column was always less than 250 mV.

The higher corrosion rate near the influent end of the column is also reflected in the anodic Tafel scans in Figure 4c. The anodic Tafel slope for the inlet sampling port was always less that that for the middle port. This can be attributed to the presence of a greater mass of iron oxides near the column inlet that provided a greater anodic area, and thus a greater current at low anodic overpotentials, as shown in Figure 4c for potentials between –528 and –480 mV. However, at more positive potentials, the rate of Fe^{2+} generation increased sufficiently that iron oxidation became limited by the rate at which Fe^{2+} was able to enter the solution. Under these conditions, the greater oxide mass served as a greater barrier to Fe^{2+} diffusion, and thereby decreased the anodic current at the inlet relative to the middle port.

Differences in corrosion rate along the length of the column will give rise to varying k_o values, since k_o reflects the rate of adsorption site generation. Also, differences in the speciation and morphology of the iron oxides along the length of the column may give rise to variation in k_1 values. To examine this effect, the kinetic model was fit to the steady state profiles for influent As(V) concentrations between 2,500 and 23,500 μg/L. Because of differences in corrosion rates, the column was divided into two sections for independent parameter evaluation. For the section of the column between the inlet and

the first sampling port, the best-fit k_1 and k_o values were 0.25 min^{-1} and 1111 $\mu gL^{-1}min^{-1}$, respectively. For the section of the column between the first sampling port and the column outlet, the best-fit k_1 and k_o values were 0.09 min^{-1} and 92 $\mu gL^{-1}min^{-1}$, respectively. A model fit using these parameters is shown in Figure 4a.

The different rate parameters for the two sections of the column gave rise to differences in the apparent reaction order. Figure 5 shows the As(V) removal rate as a function of the average concentration for the section of the column before the first sampling port, and for the section of the column after the first sampling port. The slope of this graph yields the apparent reaction order with respect to the arsenate concentration (*107*). As shown in Figure 5, the apparent reaction order before the first sampling port was 0.69, while after the first sampling port the reaction order was only 0.38. The intermediate result between zero and first-order indicates that both mass transfer and site saturation effects were important in the column reactor. The smaller apparent reaction order downstream of port 1 indicates that site saturation effects were more important in this part of the column, despite the lower arsenate concentrations. This supports the hypothesis that removal rates were limited by iron corrosion rates.

The different k_1 values between the two sections of the column can also be attributed to differences in iron oxidation products. Analyses of both XANES and EXAFS spectra of two column samples show the presence of magnetite (Fe_3O_4) (or maghemite, which is a defect form of magnetite enriched in Fe^{3+} and containing cation vacancies (*96*)), a Fe(III) hydroxide or oxyhydroxide, and possibly a mixed Fe(II,III) hydroxide. Because these are bulk samples, the spectra represent an average of all iron phases in the reacted

iron filings, including surface phases. Magnetite and maghemite were likely present in the air-formed oxide coating the iron at the commencement of the experiments (*108*).

Figure 6a compares the first-derivative XANES spectra of samples from the influent and effluent ends of the column to best-fit linear combinations of reference compounds. The sample from the effluent end is less oxidized than that from the influent end, and contained a mixture of iron metal, magnetite, and an Fe(III) oxide phase (represented by goethite (FeOOH); however, other Fe(III) oxides and hydroxides have similar spectral features (*103*)). Mismatch between the effluent sample data and the fit from 7110-7117 eV can be attributed to the presence of iron metal (no reference spectrum was available) that is expected to have strong absorption features at lower energy because of its lower oxidation state (*109, 110*). In contrast, the influent sample spectrum shows a lack of absorption features from iron metal at these energies. It can be fit with a combination of magnetite, Fe(III) oxide, and Fe(II,III) hydroxide (freshly precipitated sample), and indicates oxidation of the original iron metal. This interpretation is also supported by the position of the pre-edge absorption peak for the influent and effluent samples (Fig. 6a, inset). Maximum pre-edge adsorption is higher in the influent sample than in the effluent sample, which is consistent with an average higher oxidation state for iron. Pre-edge peaks in both column samples are similar to pre-edge peak positions in reference mixtures of Fe(II), Fe(III), and Fe (II,III) oxide reference compounds (when corrected for differences in calibration energy) (*110*).

Interatomic distances determined from EXAFS analyses are also consistent with a mixture of iron metal, magnetite, and a Fe(III) oxide (Fig. 6b and Table 2). Interatomic

Fe-Fe distances in the effluent sample attributed to scattering in iron metal are found at very short distances (2.49 Å and 2.89 Å) and between 4-5 Å (Table 2). These backscattering atoms are strong in the less oxidized effluent sample spectrum (Fig. 6b). First-neighbor oxygen atoms represent a mixture of magnetite, in which iron is both 4- and 6-coordinated by oxygen atoms, and Fe(III) oxide, in which iron is 6-coordinated. Iron backscattering at 2.97 Å and 3.48 Å is characteristic of magnetite. Another shell of iron atoms at ~3.10 Å does not correspond to crystallographic distances in either iron metal or magnetite, but is consistent with interatomic distances in Fe(III) hydroxides and oxyhydroxides (*94, 103*). In the more oxidized influent sample, backscattering from iron metal and magnetite is diminished and stronger backscattering from iron atoms at 3.06 Å is observed (Fig. 6b), suggesting a greater proportion of the Fe(III) oxide phase. Interatomic Fe-Fe distances in the range of ~3.0-3.1 Å are typical for edge sharing of Fe(III) octahedra in oxide and phyllosilicate phases. Iron(II) hydroxide ($Fe(OH)_2$) and mixed Fe(II)/Fe(III) hydroxide phases ("green rust", pyroaurite-type double hydroxides) have second-neighbor iron atoms at slightly longer distances (~ 3.20-3.27 Å), reflecting the larger ionic radius of Fe^{2+} (*103, 110*). A small proportion of Fe(II/III) hydroxide suggested by the XANES data could not be confirmed in the EXAFS spectra due to strong scattering from second-neighbor iron atoms in the dominant phases, but it may form under these solution conditions as a metastable intermediate (*96, 110*).

Effluent arsenate concentrations for the stainless steel column are shown in Figure 7a, and the history of the column is summarized in Table 3. Arsenate removal to below the detection limit was observed for an influent concentration of 100 µg/L and a hydraulic

residence time of 20 seconds. The removal below 1 μg/L was observed for more than 500 pore volumes until the hydraulic residence time was changed to 25 minutes. With a residence time of 25 minutes, removal below 1 μg/L was observed for 220 days (12,600 pore volumes). At 220 days the influent concentration was increased to 5,000 μg/L, and the resulting effluent concentration increased to ~1,000 μg/L, as shown in Figure 7a.

A feed concentration of 5,000 μg/L was not maintained for a sufficient period of time to reach steady state removal. However, at feed concentrations of 10,000 and 15,000 μg/L, approximate steady state removal was observed for a period of 75 days (4,300 pore volumes), between 230 and 305 days elapsed. Not only was steady state achieved, but the C/C_o values were approximately the same for feed concentrations of 10,000 and 15,000 μg/L. The similar C/C_o values are consistent with pseudo-first-order removal, and suggest that removal rates were limited by mass transfer limitations. This contrasts with the behavior after 305 days elapsed where there was no increase in removal when the influent concentration was increased from 15,000 to 20,000 μg/L, as shown in Figure 7b. This is consistent with pseudo-zeroth order removal kinetics.

The switch between pseudo-first and pseudo-zeroth order kinetics can be attributed to a shift from an excess to a shortage of adsorption sites. At low influent concentrations the rate of adsorption site generation was greater than the rate at which sites were being occupied by arsenate. This resulted in an excess of unoccupied adsorption sites. With increasing arsenate concentration, the rate of site depletion eventually became greater than the rate of site generation. This resulted in a loss in the number of available sites, and increasing competition for adsorption sites over time. The declining removal rates

shown in Figure 7b for feed concentrations above 20,000 µg/L is consistent with a depletion in the number of available sites with increasing elapsed time.

The sustained performance of zerovalent iron for arsenic removal is dependent on the continuous generation of iron oxide adsorption sites, and on the ability of arsenic to reach adsorption sites via diffusion. The iron corrosion products formed in this study using waters with low levels of dissolved oxygen appear to be sufficiently porous to allow arsenic diffusion to adsorption sites. Furthermore, for low As(V) concentrations, iron corrosion rates appear to be sufficiently fast to produce adsorption sites more rapidly than they become occupied by adsorbed arsenic. However, competition for adsorption sites by other anions that form complexes with iron oxides, such as phosphate and silicate, may lead to a shortage of available sites for arsenic adsorption. In that case, it may be necessary to increase the rate of adsorption site generation by adding oxygen to the water. Although higher levels of dissolved oxygen will promote faster iron corrosion, the resultant thicker oxide layers may lead to greater mass transfer resistance for arsenic removal. Additionally, the morphology and porosity of the iron oxides may be adversely affected by higher rates of iron corrosion in more aerobic waters (*96*, *111*). More research is needed to resolve these issues in order to design effective treatment schemes employing zerovalent iron media.

4.5 Acknowledgements

Thanks to Wayne Seames, Wendell Ela, Mike Kopplin and Ron Leblanc for assistance with the arsenic analyses, and to Rob Root and Nelson Rivera for assistance with the

synchrotron work. This project was made possible by grant number 2P42ES04940-11 from the National Institute for Environmental Health Sciences of the National Institutes for Health. Funding for synchrotron data collection was provided by the National Science Foundation, EAR-9629276 and EAR-0073984 (to O'Day). Work done (partially) at SSRL which is operated by the DOE, Office of Basic Energy Sciences.

Table 4.1 Influent and effluent As(V) concentrations for the 50 cm column operated with a mean hydraulic detention time of 20 minutes.

Days Elapsed	Influent Concentration (μg/L)	Effluent Concentration (μg/L)
0-4	100	0
4-7	500	0
7-10	1,000	0[1]
10-13	2,500	468
13-16	5,000	2140
16-19	10,000	5,539
19-23	23,500	13,558

[1] A concentration of 278 μg/L was observed at port 1.

Table 4.2 Iron K-edge EXAFS fit results[a].

	Atom	N	R(Å)	σ^2(Å^{-1})	Phase[b]
Influent End	O	5.1	2.00	0.0121	mg, ox
	Fe	0.1	2.49[c]	0.0050[c]	mt
	Fe	1.5	2.90	0.0070[c]	mg, ox?
	Fe	2.8	3.06	0.0070[c]	ox?
	Fe	0.9	3.48[c]	0.0070[c]	mg
Effluent End	O	4.2	2.01	0.0166	mg, ox
	Fe	1.5	2.49[c]	0.0050[c]	mt
	Fe	1.5	2.97[c]	0.0070[c]	mg
	Fe	1.8	3.10	0.0070[c]	ox?
	Fe	1.9	3.48[c]	0.0070[c]	mg
	Fe	2.8	4.09	0.010[c]	mt
	Fe	9.3	4.81	0.010[c]	mt

Reference Compounds:					Crystallographic Values		
	Atom	N	R(Å)	σ^2(Å^{-1})	Atom	N	R(Å)
Magnetite[d]	O	1.3	1.87	0.0015	Fe^{IV}-O	4	1.887
	O	4.0	2.03	0.0048	Fe^{VI}-O	6	2.060
	Fe	4.0	2.98	0.0073	Fe^{VI}-Fe	6	2.968
	Fe	6.0	3.48	0.0075	Fe^{VI}-Fe	6	3.480
					Fe^{IV}-Fe	12	3.480
	Fe	1.3	3.63	0.0016	Fe^{IV}-Fe	4	3.635
Iron metal[e]					Fe	8	2.486
					Fe	6	2.870
					Fe	12	4.059
					Fe	24	4.759

[a]N is the number of backscatters at interatomic distance (R); σ^2 is the Debye-Waller term (absorber-backscatterer root-mean-squared disorder).

[b]Backscattering attributed to a particular phase based on a characteristic interatomic distance (R): mt = iron metal; mg = magnetite, ox = iron oxyhydroxide.

[c]Parameter fixed in least-squares fit. R is taken from published X-ray diffraction refinements; σ^2 was estimated from EXAFS fits to reference compounds.

[d]Commercial, synthetic magnetite; structure verified by X-ray diffraction. Crystallographic R calculated from the structure refinements reported in Waychunas (*39*); N fixed in least-squares fit on the weighted average of iron in octahedral and tetrahedral sites; σ^2 was varied.

Table 4.2 ***continued*** Iron K-edge EXAFS fit results[a].

[c]Interatomic distances calculated from the structure refinement of Kittel (*40*); only single-scattering paths are shown. A large number of 3-legged multiple-scattering paths occurs at 3.921 Å.

Table 4.3 Influent and effluent As(V) concentrations for the 25 cm column operated with a mean hydraulic detention time of 25 minutes.

Days Elapsed	Influent Concentration (μg/L)	Effluent Concentration (μg/L)
0-140	100	0
140-155	300	0
155-170	600	0
170-210	1,000	0
210-220	1,500	0
220-230	5,000	1,100[1]
230-270	10,000	5,600
270-305	15,000	7,500
305-315	20,000	12,600[1]
315-335	25,000	20,000[1]
335-365	35,000	32,000[1]
365-393	50,000	49,300[1]

[1]Not steady state concentrations but averaged values over the operation time.

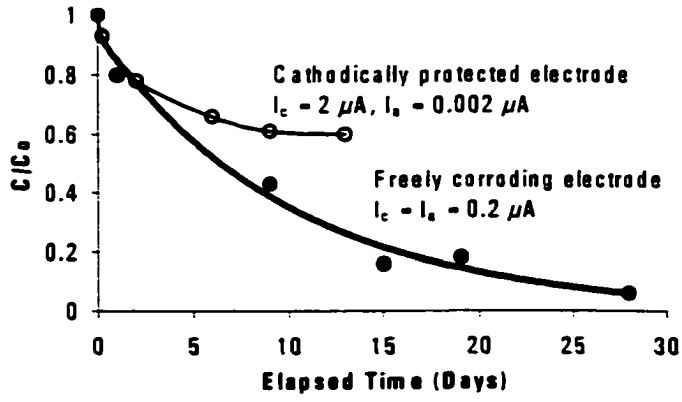

Figure 4.1 Normalized As(V) aqueous concentrations in two batch reactors with initial As(V) concentrations of 100 μg/L. Solid lines are model fits to the experimental data using equation 1.

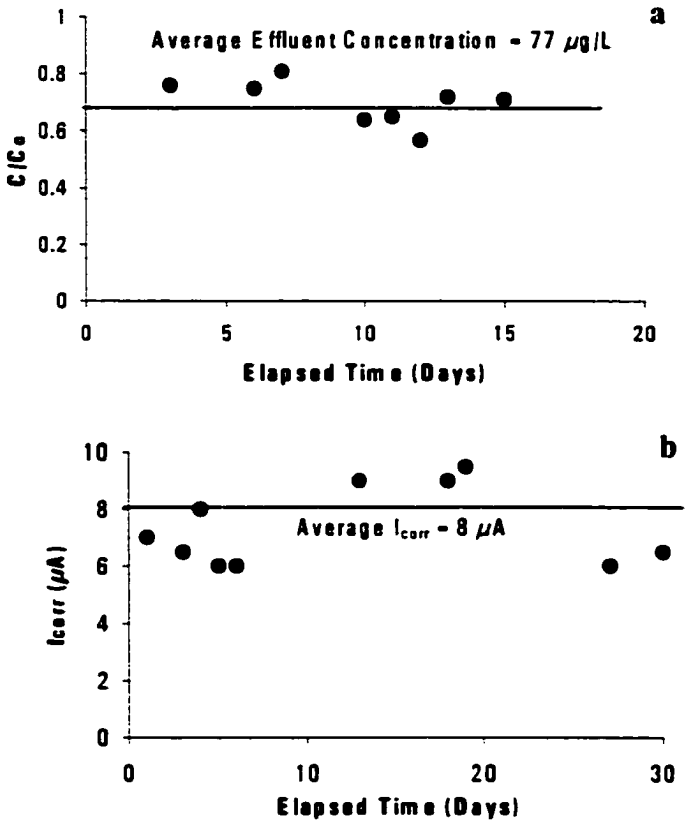

Figure 4.2 a) Effluent As(V) concentrations from the flow-through iron wire reactor for an influent As(V) concentration of 117 μg/L. The reactor was operated at a flow rate of 1 mL/min and had a mean hydraulic detention time of 250 min. b) Corrosion currents (I_{corr}) for the iron wire in the flow-through reactor.

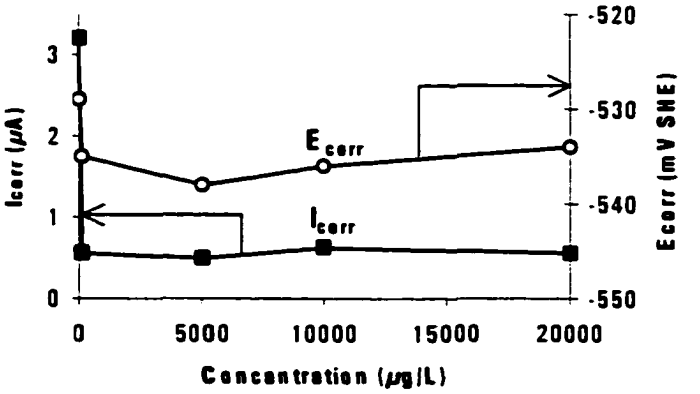

Figure 4.3 Corrosion currents (I_{corr}) and free corrosion potentials (E_{corr}) for a single 10 cm long iron wire immersed in anaerobic As(V) solutions after one day elapsed at each concentration.

Figure 4.4 a) Aqueous As(V) concentrations as a function of the hydraulic detention time in the 50 cm long column reactor packed with iron filings. The solid lines are model fits to the experimental data using equation 1 for influent As(V) concentrations between 2,500 and 23,500 μg/L. b) Corrosion currents for the iron wire probes inserted into the inlet and three intracolumn sampling ports for influent As(V) concentrations of 0 and 23,500 μg/L. c) Tafel scans for the iron wire probes inserted into the inlet and middle sampling ports.

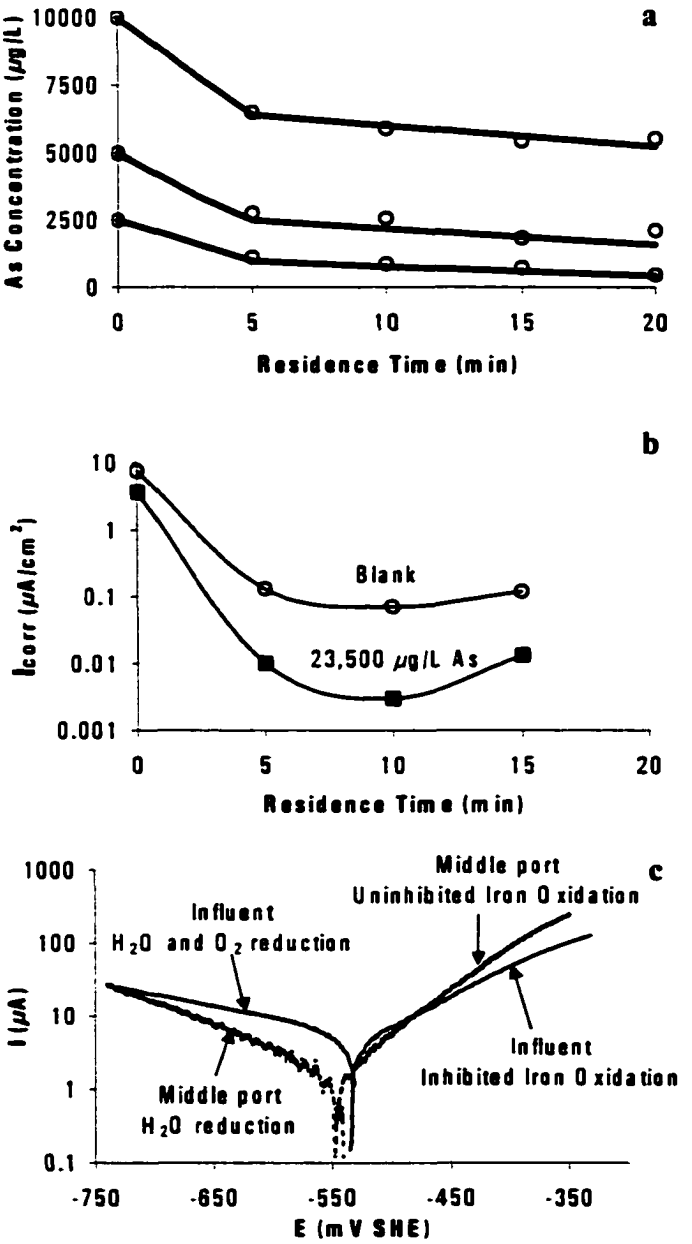
a
As Concentration (μg/L)
10000
7500
5000
2500
0
0
5
10
15
20
Residence Time (min)
b
I_{corr} (μA/cm²)
10
1
0.1
0.01
0.001
Blank
23,500 μg/L As
0
5
10
15
20
Residence Time (min)
c
I (μA)
1000
100
10
1
0.1
Influent
H_2O and O_2 reduction
Middle port
H_2O reduction
Middle port
Uninhibited Iron Oxidation
Influent
Inhibited Iron Oxidation
-750
-650
-550
-450
-350
E (mV SHE)

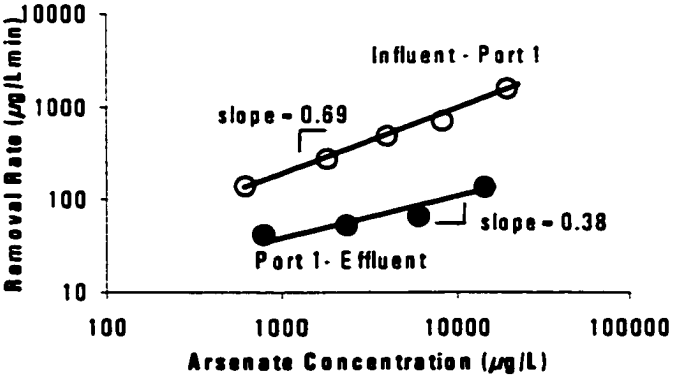

Figure 4.5 Average As(V) removal rates as a function of the average aqueous As(V) concentration for the section of the column between the inlet and the first sampling port, and for the section of the column between the first sampling port and the effluent end of the column.

Figure 4.6 a) First derivative spectra of normalized Fe K-edge XANES for reacted iron filings from the influent and effluent ends of the 25 cm column reactor (solid black) compared to reference spectra of magnetite (solid dark gray), Fe(III) oxyhydroxide (goethite; light gray), and precipitated Fe(II,III) hydroxide (dashed gray). Dashed black line is the best-fit linear combination of the reference spectra. Mismatch between data and fit for the effluent sample between 7110 and 7115 eV is attributed to the presence of iron metal (reference spectrum not available). Inset shows a blow-up of the pre-edge region of the normalized iron absorption spectrum for the column influent and effluent samples. b) Normalized EXAFS spectra for iron column samples compared to reference magnetite spectrum (x-axis uncorrected for backscatterer phase shift). Solid lines are experimental data; dashed lines are non-linear least squares fits (numerical fit results are given in Table 2). Arrows indicate strong backscattering from near-neighbor iron atoms at 2.49 Å that are indicative of iron metal.

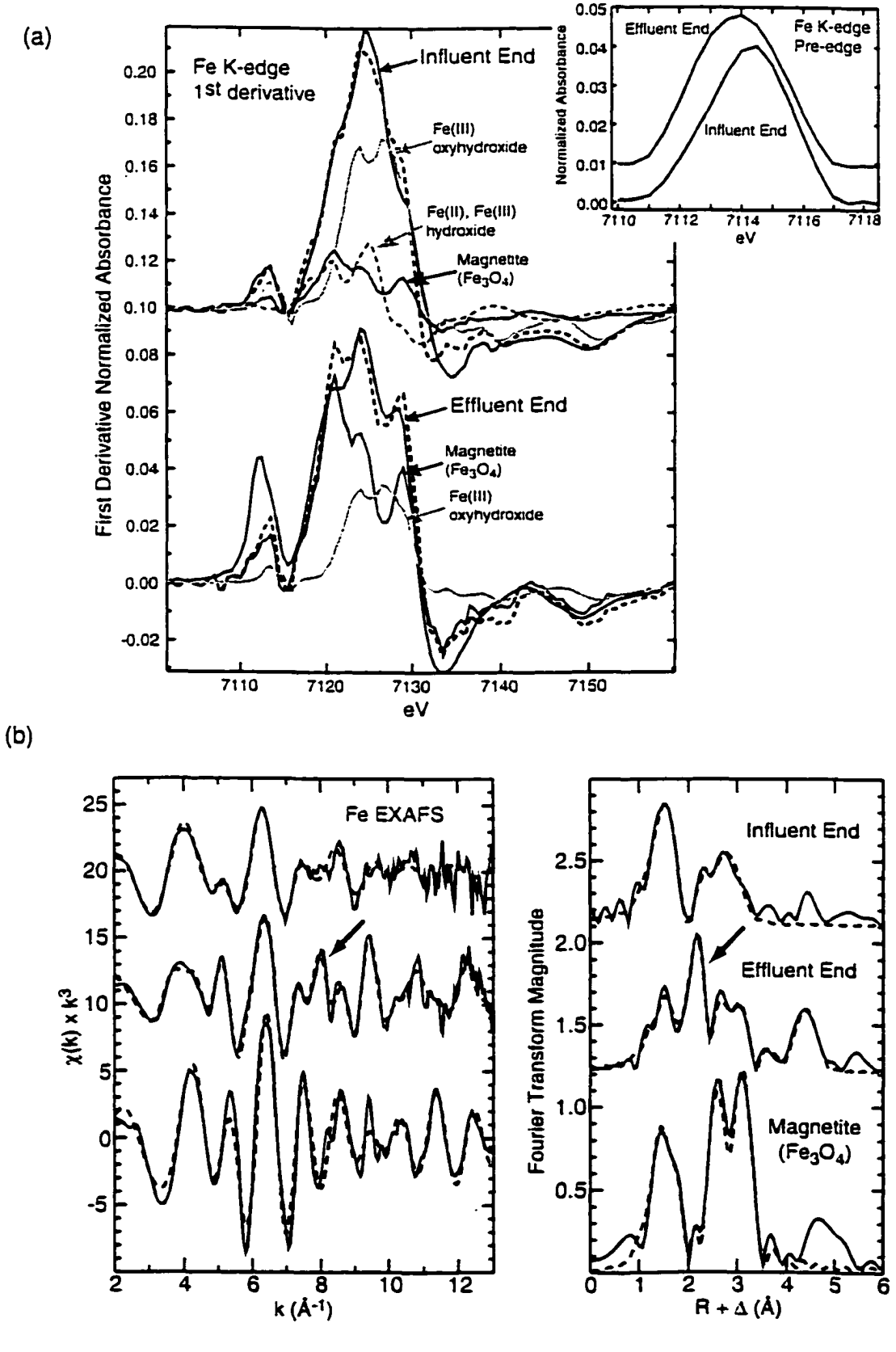
(a)
Fe K-edge
1st derivative
Influent End
Fe(III)
oxyhydroxide
Fe(II), Fe(III)
hydroxide
Magnetite
(Fe3O4)
Effluent End
Magnetite
(Fe3O4)
Fe(III)
oxyhydroxide
First Derivative Normalized Absorbance
eV
Effluent End
Fe K-edge
Pre-edge
Influent End
Normalized Absorbance
eV
(b)
Fe EXAFS
χ(k) x k3
k (Å-1)
Influent End
Effluent End
Magnetite
(Fe3O4)
Fourier Transform Magnitude
R + Δ (Å)

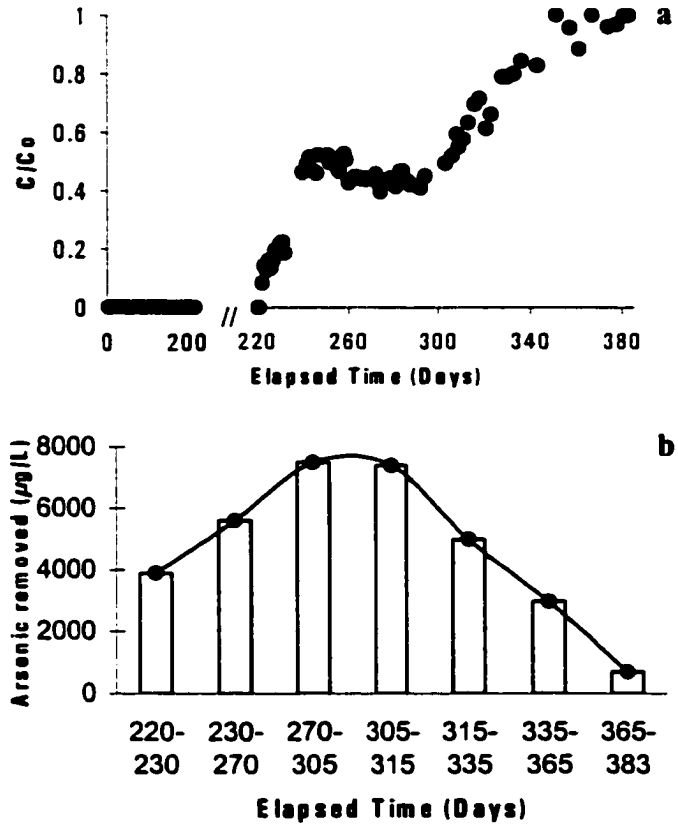

Figure 4.7 a) Normalized effluent As(V) concentrations for the 25 cm column reactor packed with iron filings. The operating conditions for the reactor are summarized in Table 3. b) Average As(V) removal by the 25 cm column reactor as a function of elapsed time.

CHAPTER 5

ELECTROCHEMICAL STUDY OF ARSENATE AND WATER REDUCTION ON IRON MEDIA USED FOR ARSENIC REMOVAL FROM POTABLE WATER

5.1 Abstract

Zerovalent iron filings have been proposed as a filter medium for removing As(III) and As(V) compounds from potable water. The removal mechanism involves complex formation of arsenite and arsenate with the iron surface and with iron oxides produced from iron corrosion. There is conflicting evidence in the literature on whether As(V) can be reduced to As(III) by iron filter media. This research uses electrochemical methods to investigate the redox reactions that occur on the surface of zerovalent iron in arsenic solutions. The effect of arsenic on the corrosion rate of zerovalent iron was investigated by analysis of Tafel diagrams for iron wire electrodes in anaerobic solutions with As(V) concentrations between 100 and 20,000 μg/L. As(V) reduction in the absence of surface oxides was investigated by analysis of chronoamperometry profiles for iron wire electrodes in solutions with As(V) concentrations ranging from 10,000 to 10^6 μg/L. The effect of pH on As(V) reduction was investigated by analyses of chronopotentiometry profiles for iron wire electrodes at pH values of 2, 6.5, and 11. For freely corroding iron, the presence of As(III) and As(V) decreased the iron corrosion rate by a factor of five compared to that in a 3 mM $CaSO_4$ blank electrolyte solution. The decrease in corrosion rate was independent of the arsenic concentration, and was due to the blocking of cathodic sites for water reduction by arsenic compounds chemisorbed to the iron surface. The chronoamperometry and chronopotentiometry experiments showed that elevated pH

and increased As(III) to As(V) ratios near the iron surface decreased the thermodynamic favorability for As(V) reduction. Therefore, reduction of As(V) occurred only at potentials that were significantly below the apparent equilibrium potentials based on bulk solution pH values and As(III) to As(V) ratios. The potentials required to reduce more than 1% of the As(V) to As(III) were below those that are obtainable in freely corroding iron media. This indicates that there will be minimal or no reduction of As(V) in iron media filters under conditions relevant to potable water treatment.

5.2 Introduction

The recent discovery of widespread arsenic contamination in potable water supplies in developing nations has brought new attention to the problem of arsenic in drinking water. In the United States, the Environmental Protection Agency has recently proposed to lower the maximum contaminant level of arsenic in drinking water from 50 to 10 μg/L (*112*). The increased attention on arsenic toxicity has incited considerable research for developing new methods of removing arsenic compounds from potable water. One new method for arsenic removal employs filter media containing zerovalent iron (*113-118*).

Several investigators have reported that iron filter media removes As(V) (arsenate) and As(III) (arsenite) compounds via mono- and bidentate complex formation of the arsenic species with iron oxides produced from iron corrosion (*113-115*). In the limit of infinite dilution of adsorbing species with respect to the number of adsorption sites, arsenic removal is limited by mass transfer to adsorption sites, and is therefore first order in arsenic concentration (*114, 119*). In the limit of high solution concentrations, arsenic

removal becomes limited by the rate of adsorption site generation, and is therefore zeroth order in arsenic concentration (*114, 119*).

The issue of arsenic redox reactions in iron filter media has not been resolved. Several investigations using column reactors packed with iron filings have reported that the relative concentrations of As(V) to As(III) in the effluent solutions were the same as those in the feed solutions *(113, 119)*. Spectroscopic analyses of iron filings from column reactors treating As(V) have found no discernable As(III) or As(0) associated with the iron particles, even after more than one year of operation (*114*). These observations suggest that there is no reduction of As(V) in iron media filters.

Although column studies have not observed changes in the arsenic oxidation state, reduction of As(V) and oxidation of As(III) has been observed in batch experiments conducted in sealed vials containing iron filings (*115*). Su and Puls reported that the ratio of As(V) to As(III) on iron filings after 60 days elapsed was approximately 1 to 3. This ratio was independent of whether As(V) or As(III) was the initial reactant, which strongly suggests that the 1 to 3 ratio is representative of equilibrium between As(V) and As(III) on the iron surfaces.

The issue of As(V) reduction and As(III) oxidation in iron filter media is important because As(III) exhibits different binding characteristics than As(V). The relative binding strength of As(III) versus As(V) depends on the type of iron oxide, the solution pH, and the solution concentration of each species *(120-123)*. For example, As(V) is more strongly bound to ferrihydrite and goethite at subneutral pH values, while there is stronger binding of As(III) to these iron oxides at neutral to alkaline pH values (*120-*

1233). Thus, understanding the arsenic redox chemistry is important since transformation of arsenic from an oxidation state that is more strongly bound to one that is less strongly bound may lead to release of arsenic from the filter media.

The equilibrium potential for the As(III)/As(V) redox couple depends on the relative concentrations of As(III) and As(V), and on whether reduction occurs to bound or solution phase arsenic species. For the As(III) and As(V) species that are expected to predominate under the pH conditions near the surface of freely corroding iron (*i.e.*, pH ≈ 9.5 (*124*)), reduction of As(V) may be described by:

$$HAsO_4^{2-} + 3H^+ + 2e^- \rightarrow AsO_2^- + 2H_2O \qquad (1)$$

The equilibrium potential (E_{eq}) for this reaction at 25 °C is given by (*125*):

$$E_{eq} = 0.609 - 0.0887\ pH + 0.0295 \log \frac{[HAsO_4^{2-}]\ \gamma_{As(V)}}{[AsO_2^-]\ \gamma_{As(III)}} \qquad (2)$$

where $[HAsO_4^{2-}]$ and $[AsO_2^-]$ are the molar concentrations of each species, and $\gamma_{As(V)}$ and $\gamma_{As(III)}$ are the activity coefficients of the As(V) and As(III) species, respectively. The relative concentrations of As(III) and As(V) at the iron surface will depend on their bulk solution ratio, and on the difference in potential between the iron surface and the bulk solution (ψ_s). For an As(III) compound with a charge of m, and an As(V) compound with a charge of n, the ratio of As(III) to As(V) at the iron surface is given by:

$$\left[\frac{As(III)}{As(V)}\right]_{surface} = \left[\frac{As(III)}{As(V)}\right]_{bulk} \exp\left[\frac{(n-m)F\psi_s}{RT}\right] \qquad (3)$$

If reduction occurs to As(V) species that are bound to the iron surface or to iron oxides, differences in binding strength between As(III) and As(V) will affect the equilibrium

potential for the redox couple. Figure 1 illustrates how differences in binding strength leads to differences in standard reduction potentials (E^o) for free and bound As(V) species. For example, stronger binding of As(III) means that $\Delta G_2^o > \Delta G_4^o$, and thus $E_3^o > E_1^o$. Therefore, bound As(V) will be reduced at higher potentials than aqueous arsenate.

This research investigated the electrochemical reactions that occur on the surface of zerovalent iron media in arsenate solutions. Tafel polarization diagrams were analyzed to determine the contributions of hydrogen evolution and As(V) reduction to the overall rate of iron corrosion. Chronoamperometry and chronopotentiometry experiments were performed using iron wire cathodes to investigate the potential and pH conditions necessary for reduction of adsorbed and solution phase As(V).

5.3 Materials and Methods

5.3.1 Batch Reactors

All experiments were performed in sealed glass reactors in 3 mM $CaSO_4$ background electrolyte solutions at neutral pH, except where otherwise noted. As(V) concentrations were controlled by adding ACS reagent, 99.7% assay, Na_2HAsO_4 (Sigma, St. Louis, MI) to the background electrolyte solutions. Ion chromatography analyses showed that As(III) was an impurity in the Na_2HAsO_4 at a level of 1%; therefore, all starting solutions possessed an As(V) to As(III) ratio of 100 to 1.

To assess the effect of arsenic concentration on the rate of iron corrosion, a single 10 cm long iron wire of 99.9% purity (Aesar, Ward Hill, MA) was placed in 0.75 L of a 3 mM

$CaSO_4$ electrolyte solution in the glass reactor containing a calomel reference electrode and a stainless steel counter electrode. The solution was continuously purged with 50 mL/min of humidified nitrogen gas in order to exclude dissolved oxygen and to mildly agitate the solution. After one week in the blank electrolyte solution, the corrosion rate of the iron had stabilized and sodium arsenate was added to the reactor through the vent tubing to produce dissolved As(V) concentrations ranging from 100 to 20,000 μg/L. The wire was exposed to each concentration for one day, at which point a Tafel scan was performed to determine the iron corrosion rate (*114*).

Chronoamperometry experiments were performed to assess the effect of potential and As(V) concentration on arsenate reduction. Chronoamperometry measures the current associated with a fixed electrode potential as a function of time (*126*). These experiments utilized a 3.5 cm long iron wire immersed in 15 mL of electrolyte solution in a glass electrochemical cell (EG&G, Oak Ridge, TN). Upon immersion of the iron wire in the electrolyte solution, a potential of –2,000 mV with respect to the standard hydrogen electrode (SHE) was applied for one minute in order to reduce any air formed oxides present on the iron. The potential was then changed to –885 mV/SHE and the resulting current was monitored as a function of time. Once the current reached a steady value, arsenate was added to produce concentrations of 10^4, 10^5 or 10^6 μg/L. After 10 minutes elapsed the potential was further lowered to –1,385 mV/SHE.

Chronopotentiometry experiments were performed to assess the effect of As(V) concentration, current density, and pH on arsenate reduction. Chronopotentiometry measures the potential associated with a fixed current as a function of time (*126*). In

these experiments, a 3.5 cm long iron wire was immersed in 15 mL of electrolyte solution in a glass electrochemical cell. After immersion of the electrode, a constant cathodic current was applied and the resulting potential was monitored as a function of time until the potential reached a steady value. Chronopotentiometry profiles were recorded at constant pH values of 2, 6.5, and 11 at fixed currents of 0.5, 1, 5, 10, 20, 30, and 50 μA.

Both the chronoamperometry and chronopotentiometry experiments used a Hg/Hg_2SO_4 reference electrode and a platinum wire counter electrode. The platinum anode was covered with a Nafion membrane to prevent oxidation of any As(III) in solution. The reaction cells were purged with humidified nitrogen gas at a rate of 20 mL/min in order to agitate the solutions and maintain anaerobic conditions. The pH values were determined using pH test paper (Micro Essential Laboratory, Brooklyn, NY) and were adjusted by the addition of H_2SO_4 or NaOH. There were no detectable changes in pH over the course of any experiments.

5.3.2 Analytical Methods

Total arsenic concentrations in the aqueous phase were determined with a graphite furnace atomic absorption (AA) spectrophotometer (Perkin Elmer, San Jose, CA) using a published method (*127*). The oxidation state of the aqueous arsenic species was determined via ion chromatography (IC) using an atomic fluorescence detector (PS Analytical, Kent, UK). The detection limits for the AA and IC methods (*128*) were both ~1 μg/L. Corrosion currents (I_{corr}) and free corrosion potentials (E_{corr}) were measured by analysis of Tafel diagrams produced by polarizing the iron wire electrodes ±200 mV with respect to their open circuit potentials (*129*). The polarization experiments were

performed using an EG&G model 273A scanning potentiostat and EG&G M270 software. All potentials are reported with respect to the standard hydrogen electrode.

5.4 Results and Discussion

The effects of arsenic on the cathodic and anodic reactions were assessed by analysis of Tafel diagrams for an iron wire electrode in solutions containing As(V) and As(III) at a molar ratio of 100 to 1. Figure 2a shows Tafel diagrams for an iron wire exposed to As(V) concentrations ranging from 0 μg/L to 20,000 μg/L. The currents shown in Figure 2a represent the net sum of the cathodic (I_c) and anodic (I_a) currents. The I_c and I_a at each potential (E) depend on the cathodic (I_c^o) and anodic (I_a^o) exchange currents, and the equilibrium potential for the cathodic (E_{eq}^c) and anodic (E_{eq}^a) reactions according to (*129*):

$$I_c = I_c^o\left[e^{-\beta_c(E-E_{eq}^c)}\right] \tag{4}$$

$$I_a = I_a^o\left[e^{\beta_a(E-E_{eq}^a)}\right] \tag{5}$$

where β_c and β_a are the cathodic and anodic Tafel slopes, respectively. The exchange currents depend on the electroactive surface area and the concentrations of electroactive species at the electrode surface. The Tafel slopes are indicative of the specific cathodic and anodic reactions that occur on the electrode surface. Since the Tafel slope is proportional to the fraction of the applied overpotential (E-E_{eq}) that goes towards overcoming the chemical activation energy for the reaction, higher Tafel slopes indicate more chemically facile reactions (*129*).

The cathodic slopes of 0.007 dec/mV in the blank and arsenic solutions in Figure 2a indicate that water was the primary oxidant, and that arsenate reduction was insignificant at all As(V) concentrations. The lower cathodic currents at each potential in the four arsenic solutions indicate that the presence of As(V) and/or As(III) decreased the I_o^c for water reduction. At all arsenic concentrations, the I_o^c was decreased by a factor of ~5 as compared to the blank electrolyte solution. The observed decrease in I_o^c can be attributed to the blocking of cathodic sites for water reduction by adsorbed arsenic compounds. The absence of a concentration effect for As(V) concentrations between 100 and 20,000 μg/L can be attributed to saturation of the adsorption sites at a concentration of only 100 μg/L.

Several lines of evidence indicate that the blocked sites for water reduction involved chemisorbed As(V) or As(III), rather than electrostatically adsorbed compounds. At an As(V) concentration of 100 μg/L, $HAsO_4^{2-}$ makes up only 0.044% of the anions in the $CaSO_4$ electrolyte solution, and thus SO_4^{2-} should dominate over $HAsO_4^{2-}$ for electrostatic adsorption sites. However, increasing the $HAsO_4^{2-}$ concentration should increase the contribution of $HAsO_4^{2-}$ to the total amount of electrostatic adsorption. Since all As(V) concentrations exhibited the same blocking effect on water reduction, an electrostatic blocking mechanism can be ruled out.

Evidence for electroactive site blocking by chemisorbed As(V) or As(III) can also be seen in the free corrosion currents shown in Figure 2b. The factor of ~5 lower current in the arsenic solutions compared to the blank solution indicates that there was a factor of ~5 decrease in the I_o^c for water reduction. The similar decrease in I_o^c under polarized

(Figure 2a) and unpolarized conditions (Figure 2b) proves that the site blocking was not due to electrostatic adsorption, since there were different electrostatic charges on the electrode under polarized and unpolarized conditions (*129*).

The presence of arsenic compounds also affected the iron oxidation reaction, as indicated by the anodic Tafel scans in Figure 2a. The anodic scans can be divided into two regions by the potential where the slope changes at approximately -475 mV. For potentials lower than -475 mV, the β_a values in the four arsenic solutions were similar to that in the blank solution. The β_a value of 0.016 dec/mV is characteristic of zerovalent iron oxidation (*130*). Although the β_a values were the same, the lower anodic currents at each potential in the As(V) solutions indicate that the presence of arsenic decreased the I_a^o. At a potential of approximately -475 mV the β_a in all arsenic solutions began to change. This change in slope may be attributed to oxidation of iron complexed with As(III) or As(V), or to oxidation of As(III) chemisorbed to the iron surface.

The decrease in I_a^o can be attributed to the blocking of anodic sites by adsorbed arsenic compounds. Addition of only 100 µg/L arsenate resulted in a 60% decrease in I_a^o as compared to the blank solution. Since the I_a^o is proportional to the anodic area, this suggests that there was a 60% decrease in the electroactive surface area for iron oxidation. Increasing the arsenate concentration to 5,000 µg/L resulted in a further decrease of 20% in anodic current, and the presence of 20,000 µg/L As(V) lowered the anodic current by an additional 18%.

The absence of detectable As(V) reduction in the cathodic Tafel scans may be attributable to several possible phenomena. Even at potentials as low as -740 mV, it may

not have been thermodynamically favorable for As(V) reduction. Alternatively, the rate of arsenate reduction may have been too slow to be detected amperometrically, or reduction was impeded by an oxide film on the iron that blocked electrical contact of solution species with the metal surface. To distinguish among these possible explanations, chronoamperometry and chronopotentiometry experiments were performed to determine the conditions favoring As(V) reduction.

To determine if As(V) reduction would occur in the absence of an oxide coating on the iron wire, chronoamperometry experiments were performed using iron cathodes at potentials of -885 and –1,385 mV. Since these potentials are in the stability domain of zerovalent iron, the oxide coating on the iron was eliminated. However, the outer layer of iron atoms were still hydroxylated (*131*), and therefore may contain chemisorbed As(V) or As(III) species.

Figure 3a shows chronoamperometry profiles for an iron wire cathode at an applied potential –885 mV. For solutions with final concentrations of 10^4 and 10^5 μg/L, As(V) was added to each solution at the indicated concentration at 5.5 minutes elapsed. In the solution with a final concentration of 10^6 μg/L, the As(V) was added in three increments at 5.5, 5.8 and 6.1 minutes elapsed. Upon addition of arsenic to the reactors, the currents in all three As(V) solutions declined to below that of the blank. This can be attributed to the blocking of cathodic sites for water reduction by adsorbed arsenic compounds. The blocking of cathodic sites in the absence of an oxide layer indicates that As(V) or As(III) may bind to the metal surface itself.

In contrast to the decline in current in the 10^4 and 10^5 μg/L solutions, the current sharply increased in the reactor with the highest As(V) concentration once the solution concentration reached its final value of 10^6 μg/L. The increase in current was short-lived, and the current soon fell to a level below that in the blank solution. The fact that the current in the 10^6 μg/L solution dropped to that in the 10^5 μg/L solution after 5 minutes suggests that there was no sustained reduction of solution phase As(V). Additionally, despite the current pulse in the 10^6 μg/L reactor, there was no detectable increase in the solution concentration of As(III). These observations indicate that the pulse of current in the 10^6 μg/L solution can be attributed to reduction of As(V) that was chemisorbed to the iron surface. A similar reduction mechanism that first requires surface complexation has been previously observed for pertechnetate (TcO_4^-) reduction by magnetite (*132, 133*). The absence of a discernable reduction pulse in the 10^4 and 10^5 μg/L solutions suggests that As(V) reduction was insignificant. This was confirmed by aqueous As(III) concentrations that declined over the course of these experiments.

To determine if lower potentials could lead to reduction of solution phase As(V), the potential in the chronoamperometry experiment was decreased to −1,385 mV at 10 minutes elapsed. As shown in Figure 3b, the decrease in potential resulted in a sustained increase in current in the 10^6 μg/L solution. The sustained increase in current over that in the blank solution indicates reduction of dissolved As(V). This was confirmed by an increase in the solution phase concentration of As(III).

Upon lowering the potential to −1,385 mV, a current increase was also observed in the 10^5 μg/L solution, but there was no surge in current in the 10^4 μg/L solution, as shown in

Figure 3b. The current pulse in the 10^5 μg/L solution can be attributed to reduction of As(V) that was bound to the iron surface. However, the current in the 10^5 μg/L solution was never greater than that in the blank, indicating that the decrease in the current for water reduction was more significant than the current increase due to As(V) reduction. The absence of reduction in the 10^4 and 10^5 μg/L solutions at -885 mV suggests that As(V) reduction was not thermodynamically favorable at that potential for the As(III)/As(V) ratio on the iron surface. Although the bulk solution ratio of As(V) to As(III) was 100 to 1, the relative concentrations bound to the iron surface may have been significantly different. In the absence of specific adsorption, the potential for zero charge on iron surfaces is –500 mV (*129*). Therefore, at an electrode potential of –885 mV, the iron surface was negatively charged with respect to the bulk solution. The value of ψ_s depends on whether there was specific adsorption of anions or cations to the iron surface; but in the absence of specific adsorption, ψ_s was –385 mV. Specific adsorption of anionic species decrease ψ_s to a value more negative than –385 mV, while specific adsorption of cationic species increase ψ_s. For the solutions in this investigation, the compounds capable of specifically adsorbing to iron are either uncharged or negatively charged. Therefore, at a potential of –885 mV, the ψ_s is this study was most certainly below –385 mV. For the arsenic species depicted in equation1, equation 3 indicates that a ψ_s of –385 mV increases the As(III)/As(V) ratio at the iron surface by a factor of 4 x 10^6 compared to that in the bulk solution. The effect of ψ_s on the ratio of the arsenic species that predominate at neutral pH values (*i.e.*, $HAsO_2$ and $H_2AsO_4^-$) is also increased by this same factor. Thus, although the molar ratio of As(III) to As(V) in the bulk

solution was only 0.01, the ratio at the iron surface may have been more than 4 x 10^4. This analysis showing that electrostatic effects may have favored selective adsorption of As(III) over As(V) at the iron surface was confirmed by measurements of solution phase concentrations of As(III). In all chronoamperometry experiments at –885 mV, final solution concentrations of As(III) were less than initial concentrations; and in the 10^4 μg/L solution, the As(III) was completely removed.

The hypothesis that the negatively charged iron surface impeded As(V) reduction by favoring selective adsorption of As(III) was confirmed by investigating the effect of ionic strength on As(V) reduction. The fact that there was As(V) reduction in the 10^6 μg/L solution but not in solutions with lower concentrations can be attributed to the effect of a higher ionic strength on the relative concentrations of As(III) and As(V) in the solution adjacent to the electrode surface. A higher ionic strength decreases the magnitude of the charge at the outer Helmholtz plane (*134*), and thereby decreases the ratio of As(III) to As(V) in the solution adjacent to the electrode surface. This hypothesis was confirmed by the data in Figure 3c which shows that at a higher ionic strength, addition of 10^5 μg/L of arsenic resulted in a current pulse indicative of reduction of bound As(V).

The effect of pH on As(V) reduction was investigated using chronopotentiometry. Figure 4 shows steady state potentials associated with fixed cathodic currents at different arsenate concentrations at pH values of 2, 6.5, and 11. For cathodic currents above ~3 μA in the pH 2 solutions, the potentials in the As(V) solutions were lower than those in the blank electrolyte solution. However, the β_c values were approximately the same (0.0081 to 0.0084 dec/mV), indicating that hydrogen evolution was the predominant

cathodic reaction in all solutions. This shows that lower potentials were required to maintain the same rate of water reduction in the presence of arsenic as compared to the blank solution.

The lower potentials were required due to the blocking of cathodic sites by adsorbed arsenic compounds. The blocking of cathodic sites resulted in a decrease in the I_o^c for hydrogen evolution, as illustrated by the diagram in Figure 5, where the I_o^c decreased to $I_o'^c$. In this case, the sum of the currents for As(V) reduction and hydrogen evolution at each potential were lower than those for hydrogen evolution alone in the blank solution. For a fixed current, this resulted in a decrease in the electrode potential from E to E'.

For currents smaller than ~3 μA in the pH 2 solution, the equilibrium potentials in the presence of As(V) were greater than those in the blank solution. In this potential range As(V) reduction measurably contributed to the overall cathodic current, and the current at each potential was greater than the hydrogen evolution current in the blank solution. Therefore, the equilibrium potentials at the fixed total currents were greater than those for hydrogen evolution in the blank solution, as illustrated in Figure 5. This interpretation of the chronopotentiometry experiments was confirmed by up to threefold increases in solution phase As(III) concentrations in the low pH solutions.

In the solutions with pH values of 6.5 and 11 with As(V) concentrations of 10^4 μg/L, the chronopotentiometry profiles do not indicate any As(V) reduction. The absence of As(V) reduction was confirmed by a decrease in the solution concentration of As(III) in these experiments. This shows that reduction of As(V) was not thermodynamically favorable at the final potential reached in each experiment, which was -660 mV at pH 11 and -500

mV at pH 6.5. According to equation 2, the equilibrium potential for aqueous As(III) and As(V) species at pH values of 11 and 6.5 should be –310 mV and 84 mV, respectively, based on the bulk solution As(V) to As(III) ratio of 100 to 1, and a $\gamma_{As(V)}$ of 0.63 (Debye-Hückel eqn.) at both pH values, and a $\gamma_{As(III)}$ of 0.89 at pH 11 and 1.0 at pH 6.5. The absence of reduction must then be attributed to ψ_s effects and differences in binding strength of As(V) and As(III) that control their relative concentrations at the iron surface. This conclusion is supported by the presence of As(V) reduction in the 10^6 μg/L solution at a pH value of 11. The higher ionic strength at this concentration resulted in an As(III)/As(V) ratio at the iron surface that was more favorable for reduction. The observed reduction at pH 11 shows that unfavorable pH values at the iron surface cannot solely account for the absence of As(V) reduction at lower concentrations.

The electrochemical experiments show that As(V) reduction at iron surfaces occurs only at potentials that are significantly below the apparent equilibrium potential that is based on the bulk solution pH and ratio of As(V) to As(III). The predominance of As(III) on the surface of corroding iron serves to decrease the thermodynamic driving force for reduction of bound As(V). Although solution phase As(V) may be reduced, very negative surface potentials are required in order to compensate for the potential drop between the iron surface and the adjacent solution. The absence of measurable aqueous As(V) reduction at potentials as low as -740 mV in the Tafel scans suggests that there will be little or no reduction of dissolved As(V) in freely corroding iron media, where the potentials are -550 mV and above, as indicated in Figure 2b and in previous investigations (*135*).

The conclusion that significant As(V) reduction does not occur in freely corroding iron media is not inconsistent with results from previous investigators that reported reduction of As(V) to As(III) (*115*). That prior study was conducted using sealed vials over a 60 day period. When As(III) was the original species in solution, immediate oxidation to As(V) was observed. This indicates that the iron surface potential was above the equilibrium potential of the As(V)/As(III) redox couple. In contrast, when As(V) was the original species, reduction was not observed until 30 days elapsed. The lag time before reduction was observed can likely be attributed to the time required for the corrosion potential to reach the equilibrium potential of the As(III)/As(V) redox couple. Declining corrosion potentials in sealed vials can be attributed to the buildup of hydrogen gas that lowers the equilibrium potential for water reduction. This effect has been experimentally observed by Reardon (*136*) who reported that corrosion rates in sealed containers declined by 33% over a 20 day period. As shown by equation 4, a decline in cathodic current (I_c) accompanying a decline in equilibrium potential (E_{eq}), and an in increase in exchange current (I_c^o) must be associated with a decline in electrode potential (E). Not only do lower iron potentials make As(V) reduction more favorable, but lower corrosion rates also favor As(V) reduction. Oxidation of the iron by water increases the pH in the vicinity of cathodic sites, which then increases the equilibrium potential for As(V) reduction. Thus, lower corrosion rates in closed systems make the pH conditions at the iron surface more favorable for As(V) reduction.

Studies showing reduction in closed systems but no reduction in open systems have also been reported for uranyl (UO_2^{2+}) reduction by zerovalent iron. Experiments conducted in

sealed, glass vials showed reduction of U(VI) to U(IV) on the surface of zerovalent iron (*137*). However, analysis of iron foil exposed to U(VI) solutions purged with nitrogen gas showed no detectable reduction of U(VI) to U(IV) (*138*). This suggests that small differences in redox potential and pH between open and closed systems can be important in determining contaminant fate in iron treatment media.

This study showed that bound arsenic species decrease the corrosion rate of zerovalent iron, and reduction of As(V) may occur on both oxide-free and oxide-coated iron surfaces. Reduction of bound As(V) occurs at higher potentials than reduction of aqueous arsenate. This is consistent with stronger binding of As(III) versus As(V) to the iron surfaces. The stronger binding of As(III) results in an elevated As(III) to As(V) ratio on the iron surface with respect to their bulk solution ratio. The elevated As(III) concentrations on the iron surface decrease the equilibrium potential for further As(V) reduction. The pH and potential conditions necessary for significant As(V) reduction will be difficult or impossible to achieve in an open system under freely corroding conditions. Therefore, in the absence of biological reduction, there will be little conversion of As(V) to As(III) in zerovalent iron filter media.

5.5 Acknowledgements

Thanks to Mike Kopplin and Ron Leblanc for their assistance. This project was made possible by grant number 2P42ES04940-11 from the National Institutes for Environmental Health Sciences of the National Institutes for Health, with funds from the U.S. Environmental Protection Agency.

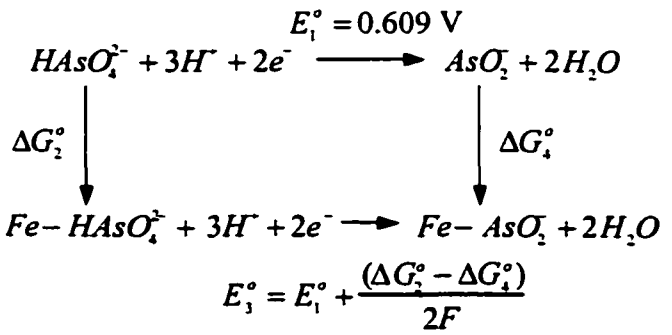

Figure 5.1 Thermodynamic cycle for reduction of aqueous and bound As(V). As(V) and As(III) may bind to the iron surface itself, and to iron oxides coating the metal surface.

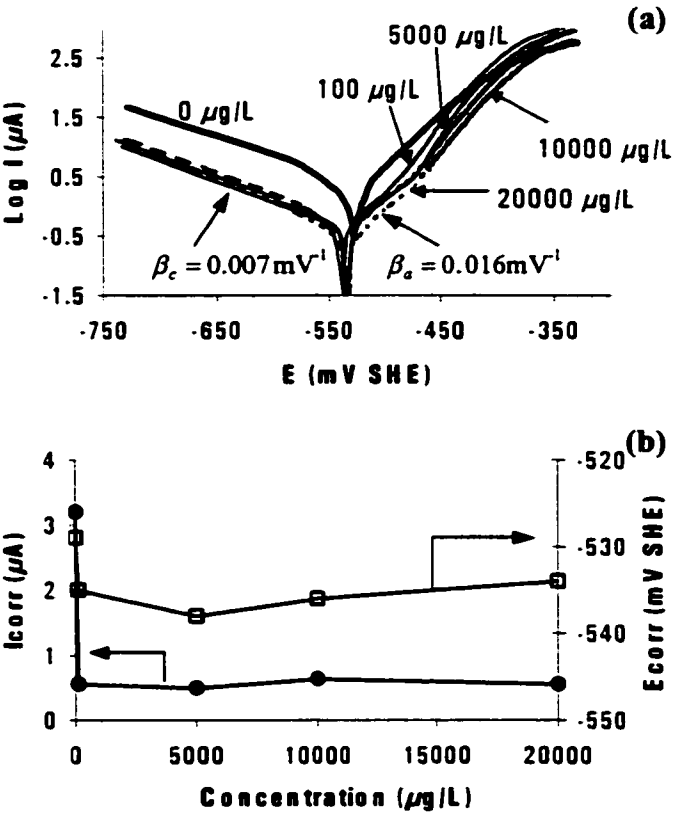

Figure 5.2 a) Tafel scans for an iron wire electrode in anaerobic 3 mM $CaSO_4$ electrolyte solutions containing As(V) at the indicated concentrations. The electrode was equilibrated with each solution for 1 day prior to performing the scan. b) Corrosion currents (I_{corr}) and free corrosion potentials (E_{corr}) determined from the Tafel scans.

Figure 5.3 a) Chronoamperometry profiles for an iron wire electrode in anaerobic 3 mM $CaSO_4$ electrolyte solutions at a potential of -885 mV. To assess the effect of dissolved oxygen in the spike solutions, 500 µL of deionized water was added to the blank solution at 5.5 minutes. The small increase in current was due to reduction of dissolved oxygen. Addition of the Na_2HAsO_4 spike solutions increased the ionic strength from 12 mM in the blank to 12.4, 16, and 52 mM in the 10^4, 10^5, and 10^6 µg/L solutions, respectively. b) Continuation of the chronoamperometry profiles after decreasing the potential from -885 to -1385 mV. c) Chronoamperometry profile at a potential of -885 mV in an anaerobic NaCl electrolyte at an ionic strength of 100 mM. At 6 minutes elapsed Na_2HAsO_4 was added to the solution to produce an As(V) concentration of 10^5 µg/L.

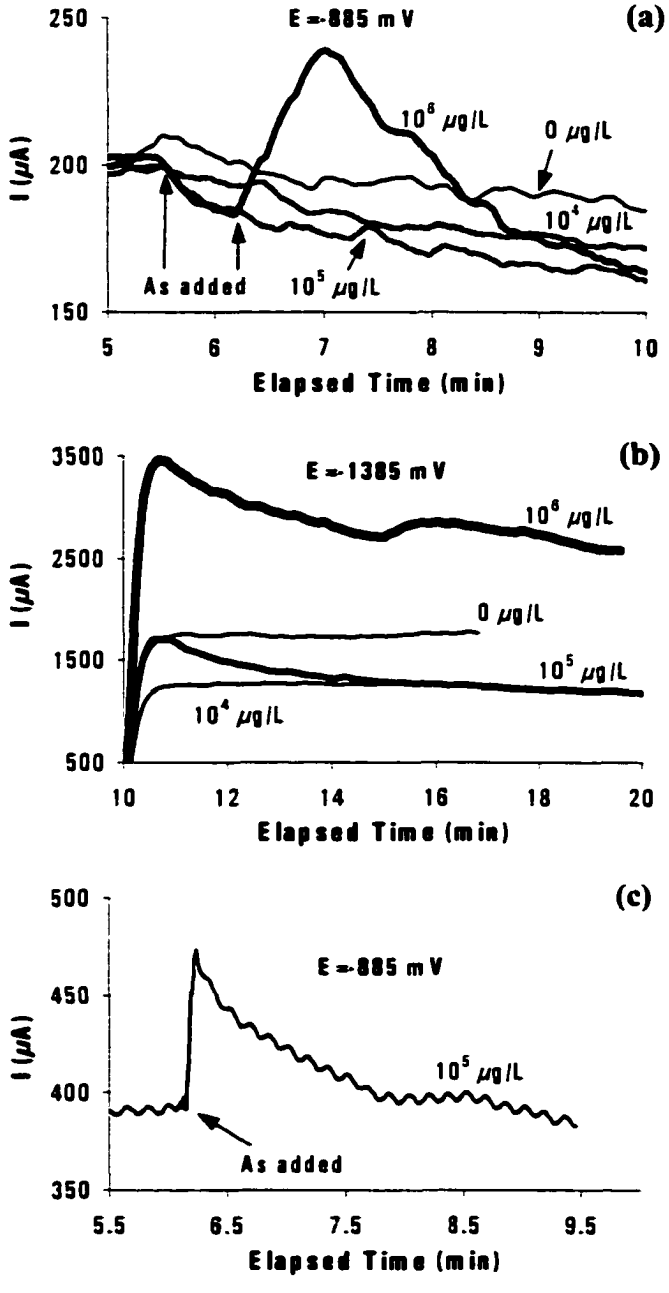
E = -885 mV
(a)
250
200
150
I (μA)
10^6 μg/L
0 μg/L
10^4 μg/L
As added
10^5 μg/L
5
6
7
8
9
10
Elapsed Time (min)
E = -1385 mV
(b)
3500
2500
1500
500
I (μA)
10^6 μg/L
0 μg/L
10^5 μg/L
10^4 μg/L
10
12
14
16
18
20
Elapsed Time (min)
(c)
500
450
400
350
I (μA)
E = -885 mV
10^5 μg/L
As added
5.5
6.5
7.5
8.5
9.5
Elapsed Time (min)

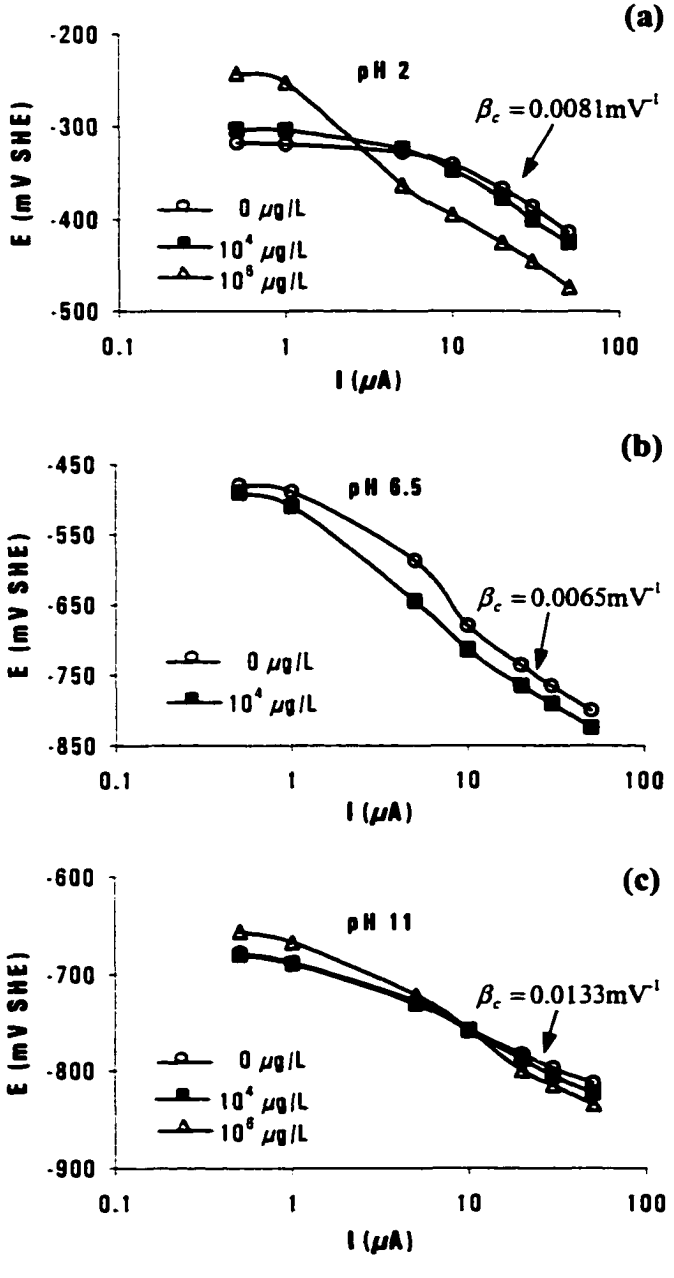

Figure 5.4 Chronopotentiometry profiles for iron wire electrodes in anaerobic 3 mM $CaSO_4$ electrolyte solutions containing As(V) at the indicated concentration at pH values of 2, 6.5, and 11.

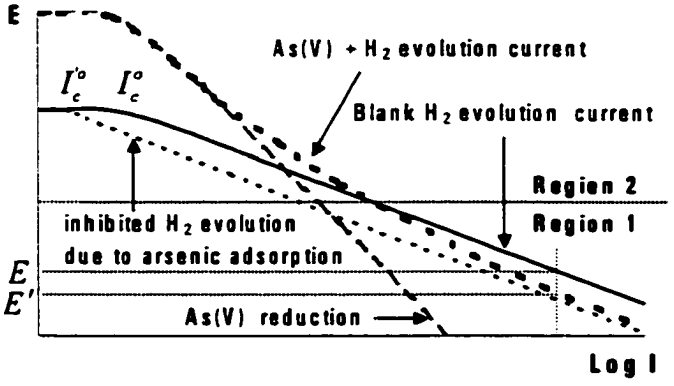

Figure 5.5 Schematic Evans diagram illustrating the effects of cathodic site blocking on the current and potential for hydrogen evolution in Region 1. Region 2 shows the effect of a measurable As(V) reduction current on the potential for simultaneous hydrogen evolution and reduction of As(V).

CHAPTER 6

CONCLUSIONS

This research showed that iron media can effectively remove chromate and arsenate from water over extended periods of time. The principal removal mechanism for chromate is reduction to Cr(III), while for arsenate the removal mechanism involves complex formation with no reduction. Although both chromate and arsenate decrease the rate of iron corrosion, chromate is a more potent passivator of the iron. For concentrations below 5,000 μg/L, the iron corrosion rate in a packed bed of filings is sufficiently fast to remove both chromium and arsenic to levels below 1 μg/L. However, higher feed concentrations overwhelm the ability of the iron to provide electrons for reduction, or adsorption sites for complexation.

At low arsenate concentrations the rate of arsenate removal is limited by diffusion of As(V) to adsorption sites. At high concentrations the rate of arsenate removal is limited by the corrosion rate which is proportional to the rate of adsorption site generation. Adsorbed arsenate blocks electroactive sites on the iron surface and decreases the corrosion rate. Arsenate is expected to remain as the principal adsorbed species since electrochemical reduction of As(V) to As(III) is not favorable at the potentials of corroding iron media.

Increasing chromium concentrations result in a decline in the removal rates due to increased passivation of the iron surface. The condition of the iron surface prior to exposure to chromate determines the kinetics of chromate removal. Air-formed oxides

significantly inhibit chromate removal whereas oxides formed in anaerobic waters result in higher removal rates. Although initial direct reduction of chromate on the iron surface was observed, with time chromate removal was limited by the rate at which Fe^{2+} is released by the corroding iron.

CHAPTER 7

REFERENCES

(1) Melitas, N.; Farrell, J.; Chuffe-Moscoso *Environ. Sci. Technol.* **2001**, 35, 3948.

(2) Melitas, N.; Farrell, J.; Wang, J. P.; Conklin, M; O'Day, P. *Environ. Sci. Technol.* **2002**, 36, 2074.

(3) Melitas, N; Farrell, J.; Conklin, M. *Environ. Sci. Technol.* **2002**, Published on the Web.

(4) *In Situ Treatment of Soil and Groundwater Contaminated with Chromium*; U. S. Environmental Protection Agency, Office of Research and Development: Washington, DC, 2000; EPA/625/R-00/005.

(5) *Technologies and Costs for Removal of Arsenic from Drinking Watrer*; U. S. Environmental Protection Agency, Office of Water: Washington, DC, 2000; EPA/815/R-00/028.

(6) Agency for Toxic Substances and Disease Registry (ATDSR). "Case Studies in Environmental Medicine, Arsenic Toxicity" U.S. Public Health Service, U.S. Department of Health and Human Services, Atlanta, GA. 1990.

(7) Waychunas, G. A.; Rey, B. A.; Fuller, C. G.; Davis, J. A. *Geochemica et Cosmochemica Acta* **1993**, 57, 15, 2251.

(8) Lackovic, J. A.; Nikolaidis, N. P.; Dobbs, G. M. *Env. Eng. Sci.* **2000**, 17(1), 29.

(9) Melitas, N.; Farrell, J.; Wang, J. P.; Conklin, M; O'Day, P. *Environ. Sci. Technol.* **2002**, 36, 2074.

(10) *Toxicology Profile for Chromium*; U.S Department of Health and Human Services, Public Health Service, Agency for Toxic Substances and Disease Registry: Washington DC, 1991.

(11) American Water Works Association *Water Quality and Treatment*, 4th ed.; McGraw and Hill Inc.:NY,1990.

(12) Kavanaugh, M. C. Alternatives for Groundwater Cleanup; National Academy Press: Washington, DC, **1994**, 315.

(13) Gillham, R. W.; O'Hannesin, S. F.; *Ground Water* **1994**, 32, 958.

(14) U.S. EPA; "Field Applications of *In Situ* Remediation Technologies: Permeable Reactive Barriers" **1999**, EPA 542-R-99-002.

(15) Powell, R. M.; Puls, W. P.; Hightower, S. K.; Sabatini, D. A. *Environ. Sci. Technol.* **1995**, 29, 1913.

(16) Blowes, D. W.; Ptacek, C. J.; Jambor, J. J. *Environ. Sci. Technol.* **1997**, 31, 3348.

(17) Patterson, R. R.; Fendorf, S.; Fendorf M.; *Environ. Sci. Technol.* **1997**, 31, 2039.

(18) Pratt, A. R.; Blowes, D. W.; Ptacek, C. J. *Environ. Sci. Technol.* **1997**, 31, 2492.

(19) Li, Z.; Jones, H. K.; Bowman, R. S.; Helferich, R. *Environ. Sci. Technol.* **1999**, 33, 4326.

(20) Astrup, T.; Stipp, S. L. S.; Christensen, T. H. *Environ. Sci. Technol.* **2000**, 34, 4163.

(21) Mayne. J. E. O.; Pryor, M. J. *J. Chem. Soc.* **1949**, 1831.

(22) Gould, J. P. *Water Res.* **1982**, 16, 871.

(23) Eary, L. E.; Rai D. *Environ. Sci. Technol.* **1988**, 22, 972.

(24) Brewster, M. D.; Passmore, R. J; *Environ. Prog.* 1994, 13, 143.

(25) Fendorf, S. E.; Li G. *Environ. Sci. Technol.* **1996**, 30, 1614.

(26) Buerge, I. J.; Hug, S. J.; *Environ. Sci. Technol.* **1997**, 31, 1426.

(27) Buerge, I. J.; Hug, S. J. *Environ. Sci. Technol.* **1998**, 32, 2092.

(28) Anderson, L. D.; Kent, D. B.; Davis, J. A. *Environ. Sci. Technol.* **1994**, 28, 178.

(29) Weng, C. H.; Huang, C. P.; Allen, H. E.; Leavens, P. B.; Sanders, P. F. *Environ. Sci. Technol.* **1996**, 30, 371.

(30) Peterson, M. L.; White, A. F.; Brown, G. E.; Parks, G. *Environ. Sci. Technol.* **1997**, 31, 1573.

(31) Buerge, I. J.; Hug, S. J. *Environ. Sci. Technol.* **1999**, 33, 4285.

(32) Loyaux-Lawniczak, S.; Refait,P.; Ehrhardt, J. J.; Lecomte, P.; Genin, J. M. R. *Environ. Sci. Technol.* **2000**, 34, 438.

(33) Deng, B.; Stone, A. T. *Environ. Sci. Technol.* **1996**, 30, 2484.

(34) Jardine, P. M.; Fendorf, S. E.; Mayes, M. A.; Larsen, S. C.; Brooks, S. C.; Bailey W. B. *Environ. Sci. Technol.* **1999**, 33, 2939.

(35) Bard, A. J.; Faulkner, L. R. *Electrochemical Methods*; John Wiley: New York, 1980.

(36) Blowes, D. W.; Gillham R. W.; Ptacek, C. J.; Puls, R. W.; Bennett, T. A.; O'Hannesin, S. F.; Hanton-Fong, C. J.; Bain, J. G. "An in situ permeable reactive barrier for the treatment of hexavalent chromium and trichloroethylene in ground water: Volume 1, Design and installation" Environmental Protection Agency. EPA/600/R-99/09.

(37) Blowes, D. W.; Puls, R. W.; Gillham R. W.; Ptacek, C. J.; Bennett, T. A.; Bain, J. G.; Hanton-Fong, C. J.; Paul C. J. "An in situ permeable reactive barrier for the treatment of hexavalent chromium and trichloroethylene in ground water: Volume 2, Performance Monitoring" Environmental Protection Agency. EPA/600/R-99/09

(38) Puls, R. W.; Paul C. J.; Powell R. M.; *Appl. Geochem.* **1999**, 14, 989.

(39) Bockris, J. O'M.; Reddy, A. K. N.; *Modern Electrochemistry*; Plenum Press: New York, 1970.

(40) Uhlig, H. H.; Revie, R. W. *Corrosion and Corrosion Control, third ed.*; John Wiley: New York, 1985.

(41) Brown, A. P.; Krumpelt, R. O.; Yao, N. P. *J. Electrochem. Soc.* **1982**, 129(11), 2481.

(42) Kreysa, G.; Hakansson, B. *J. Electroanal. Chem.* **1986**, 201, 61.

(43) Cornell, A.; Lindbergh, G.; Simonsson, D.; *Electrochim. Acta* **1992**, 37(10), 1873.

(44) Lindbergh, G.; Simonsson, D. *Electrochim. Acta* **1991**, 36(13), 1985.

(45) Bonin, P. M. L.; Odziemkowski, M. S.; Gillham, R. W.; *Corros. Sci.* 1998, 40, 1391.

(46) Odziemkowski, M. S.; Schuhmacher, T. T.; Gillham, R. W.; Reardon, E. J.; *Corros. Sci.* **1998**, 40, 371.

(47) Reardon, E. J.; *Environ. Sci. Technol.* **1995**, 29, 2936.

(48) Balko, B.; Tratnyek, P.G. *J. Phys. Chem.* B **1998**, 102, 1459.

(49) Puls, R. W.; Blowes D. W.; Gillham, R. W.; *Journal of Hazardous Materials* **1999**, 68, 109.

(50) Blowes, D. W.; Ptacek, C. J.; Benner, S. G.; McRae, C. W. T.; Bennett, T. A.; Puls R. W.; *Journal of Contaminant Hydrology* **2000**, 45, 123.

(51) *In situ treatment of soil and groundwater contaminated with chromium Environmental* ; U. S. Environmental Protection Agency, Office of Research and Development: Washington, DC, 2000; EPA/625/R-00/005.

(52) Powell, R. M.; Puls, W. P.; Hightower, S. K.; Sabatini, D. A. *Environ. Sci. Technol.* **1995**, 29, 1913.

(53) Blowes, D. W.; Ptacek, C. J.; Jambor, J. J. *Environ. Sci. Technol.* **1997**, 31, 3348.

(54) Patterson, R. R.; Fendorf, S.; Fendorf M.; *Environ. Sci. Technol.* **1997**, 31, 2039.

(55) Pratt, A. R.; Blowes, D. W.; Ptacek, C. J. *Environ. Sci. Technol.* **1997**, 31, 2492.

(56) Li, Z.; Jones, H. K.; Bowman, R. S.; Helferich, R. *Environ. Sci. Technol.* **1999**, 33, 4326.

(57) Astrup, T.; Stipp, S. L. S.; Christensen, T. H. *Environ. Sci. Technol.* **2000**, 34, 4163.

(58) Ponder, S., M.; Darab, J. G; Mallouk, T. E. *Environ. Sci. Technol.* **2000**, 34, 2564.

(59) Gould, J. P. *Water Res.* **1982**, 16, 871.

(60) Alowitz, M. J.; Scherer, M. M. *Environ. Sci. Technol.* **2002**, 36, 299.

(61) Melitas, N. T.; Farrell, J.; Chuffe-Moscoso, O. *Environ. Sci. Technol.* **2001**, 35, 3948.

(62) Bockris, J. O'M.; Reddy, A. K. N.; *Modern Electrochemistry*; Plenum Press: New York, 1970.

(63) Bard, A. J.; Faulkner, L. R.; *Electrochemical Methods*, John Wiley and Sons: New York, 1980.

(64) Tait, S. W. *An Introduction to Electrochemical Corrosion Testing for Practising Engineers and Scientists*, Pair O Docs Publications: Racine, WI, 1994.

(65) Uhlig, H. H.; Revie, R. W. *Corrosion and Corrosion Control*, 3rd ed.; John Wiley: New York, 1985.

(66) Cornell, A.; Lindbergh, G.; Simonsson, D.; *Electrochim. Acta* **1992**, 37(10), 1873.

(67) Bonin, P. M. L.; Jedral, W.; Odziemkowski, M. S.; Gillham, R. W. *Corros. Sci.* **2000**, 42, 1921.

(68) Ma, H.; Cheng, X.; Li, G.; Chen, S.; Quan, Z.; Zhao, S.; Niu, L. *Corros. Sci.* **2000**, 42, 1669.

(69) Benedetti, A. V.; Sumodjo, P. T. A.; Nobe, K.; Cabot, P. L.; Proud, W. G. *Electrochim. Acta* **1995**, 40, 2657.

(70) Evans, U. R. *An Introduction to Metallic Corrosion, 3rd ed.*; Edward Arnold: London, 1981.

(71) Bonnel, A.; Dabosi, F.; Deslouis, C.; Duprat, M.; Keddam, M.; Tribollet, B. *J. Electrochem. Soc.* **1983**, 130(4), 753.

(72) Brown, A. P.; Krumpelt, R. O.; Yao, N. P. *J. Electrochem. Soc.* **1982**, 129(11), 2481.

(73) Kreysa, G.; Hakansson, B. *J. Electroanal. Chem.* **1986**, 201, 61.

(74) Pande. S. P.; Deshpande, L. S.; Patni, P. M; Lutade. S. L. *J. Environ. Sci. Health*, **1997**, A32(7), 1981.

(75) Jain, C. K.; Ali, I. *Wat. Res.* **2000**, 17, 4304.

(76) *Federal Register* **2001**, 66, 14, 6976.

(77) Su, C.; Puls, R. W. "Retention of Arsenic by Elemental Iron and Iron Oxides," in: *Proceedings of the 1997 International Containment Technology Conference, February* 9-12, **1997**, Tallahassee, FL.

(78) Khan, A. H.; Rasul, S. B.; Munir, A. K. M.; Habibuddowla, M.; Alauddin, M.; Newaz, S. S.; Hussam, A. *J. Environ. Sci. and Health*, **2000**, A 35, 7, 1021.

(79) Alauddin, M.; Hussam, A.; Khan, A. H.; Habibuddowla, M.; Rasul, S. B.; Munir, A. K. M. Critical Evaluation of a Simple Arsenic Removal Method for Groundwater of Bangladesh, In *Proceedings of the Fourth International Conference on Arsenic Exposure and Health Hazards*, San Diego, CA, June 2000.

(80) Lackovic, J. A.; Nikolaidis, N. P.; Dobbs, G. M. *Env. Eng. Sci.* **2000**, 17, 1, 29.

(81) Farrell, J.; Wang, J. P.; O'Day. P.; Conklin, M. *Environ. Sci. Technol.* **2001**, 35, 2026.

(82) Su, C.; Puls, R. W. *Environ. Sci. Technol.* **2001**, 35, 1487.

(83) Pierce, M. L.; Moore, C. B. *Wat. Res.* **1982**, 16, 1247.

(84) Goldberg, S. *Soil Sci. Soc. Am. J.* **1986**, 5, 1154.

(85) Fuller, C. C.; Davis, J. A.; Waychunas, G. A. *Geochim. Cosmochim. Acta.* **1993**, 57, 2271.

(86) Fendorf, S.; Eick, M. J.; Grossl, P.; Sparks, D. L. *Environ. Sci. Technol.* **1997**, 31, 315.

(87) Grossl, P. R.; Eick, M.; Sparks, D. L.; Goldberg, S.; Ainsworth, C. C. *Environ. Sci. Technol.* **1997**, 31, 321.

(88) Raven, K. P.; Jain, A.; Loeppert, R. H. *Environ. Sci. Technol.* **1998**, 32, 344.

(89) Manning, B. A.; Fendorf, S. E.; Goldberg, S. *Environ. Sci. Technol.* **1998**, 32, 2383.

(90) Driehaus, W.; Jekel, M.; Hildebrandt, U. *J. Water SRT-Aqua* **1998**, 47, 30.

(91) Jain, A.; Raven, K. P. Loeppert, R. H. *Environ. Sci, Technol.* **1999**, 33, 1179.

(92) Haron, M. J.; Wan Yunus, W. M. Z.; Yong, N. L.; Tokunaga, S. *Chemosphere*, **1999**, 39, 2459.

(93) Waychunas, G. A.; Davis, J. A.; Fuller, C. C. *Geochimica et Cosmochimica Acta* **1995**, 59, 3655.

(94) Waychunas, G. A.; Rea, B. A.; Fuller, C. C.; Davis, J. A. *Geochimica et Cosmochimica Acta* **1993**, 57, 2251.

(95) Sun, X.; Doner, H. E. *Soil Science* **1998**, 163 278.

(96) Cornell, R. M.; Schwertmann, U. *The Iron Oxides*, VCH Publishers: New York, 1996.

(97) Huang, C. P.; Vane Leland M. *Journal Water Pollution Control Federation* **1989**, 61, 1596.

(98) *Test Methods for Evaluating Solid Waste*: 1986. U. S. Environmental Protection Agency, Office of Solid Waste: Washington, DC, 1986; EPA SW-846.

(99) Gregus, Z.; Gyurasics, A.; Csanaky, I. *Toxicological Sciences* **2000**, 56, 1, 18.

(100) Uhlig, H. H.; Revie, R. W. *Corrosion and Corrosion Control*, 3rd ed.; John Wiley: New York, 1985.

(101) George G. N.; Pickering, I. J. *EXAFSPAK: A suite of computer programs for analysis of X-ray absorption spectra*; Stanford Synchrotron Radiation Laboratory: Stanford, NJ, 1993.

(102) Rehr J. J.; Albers R. C.; Zabinsky, S. I. *Phys. Rev. Lett.* **1992**, 69, 3397.

(103) O'Day, P. A.; Rivera, N.; Root, R.; Carroll, S. A. Arizona State University, unpublished results.

(104) Brown, A. P.; Krumpelt, R. O.; Yao, N. P. *J. Electrochem. Soc.* **1982**, 129 (11), 2481.

(105) Kreysa, G.; Hakansson, B. *J. Electroanal. Chem.* **1986**, 201, 61.

(106) Melitas, N. M.; Chuffe-Moscoso, O.; Farrell, J. *Environ. Sci. Technol.* **2001**, 35, 19.

(107) Gould, J. P. *Water Res.* **1982**, 16, 871.

(108) Mayne, J. E. O.; Pryor, M. J. *J. Chem. Soc.* **1949**, 1831.

(109) Waychunas, G. A.; Brown, G. E., Jr.; Apted, M. J. *Physics and Chemistry of Minerals* **1983**, 10, 1.

(110) Wilke, M.; Farges, F.; Petit, P. E.; Brown, G. E., Jr.; Martin, F. *American Mineralogist* **2001**, 86, 714.

(111) Mayne, J. E. O.; Pryor, M. J.; Mentner, J. W. *J. Chem. Soc.* **1950**, 3229.

(112) *Federal Register* **2001**, 66, 14, 6976.

(113) Lackovic, J. A.; Nikolaidis, N. P.; Dobbs, G. M. *Env. Eng. Sci.* **2000**, 17(1), 29.

(114) Farrell, J.; Wang, J. P.; O'Day. P.; Conklin, M. *Environ. Sci. Technol.* **2001**, 35, 2026.

(115) Su, C.; Puls, R. W. *Environ. Sci. Technol.* **2001**, 35, 1487.

(116) Khan, A. H.; Rasul, S. B.; Munir, A. K. M.; Habibuddowla, M.; Alauddin, M.; Newaz, S. S.; Hussam, A. *J. Environ. Sci. Health* **2000**, A 35(7), 1021.

(117) Alauddin, M.; Hussam, A.; Khan, A. H.; Habibuddowla, M.; Rasul, S. B.; Munir, A. K. M. "Critical Evaluation of a Simple Arsenic Removal Method for Groundwater of Bangladesh," in: *Proceedings of the Fourth International Conference on Arsenic Exposure and Health Hazards*, June 2000, San Diego, CA.

(118) Su, C; Puls, R.W. *Environ. Sci. Technol.* **2001**, 35, 4562.

(119) Melitas, N.; Farrell, J.; Wang, J. P.; Conklin, M; O'Day, P. *Environ. Sci. Technol.* in review August 2001.

(120) Pierce, M. L.; Moore, C. B. *Water Res.* **1982**, 16, 1247.

(121) Raven, K. P.; Jain, A.; Loeppert, R. H. *Environ. Sci. Technol.* **1998**, 32, 344.

(122) Manning, B. A.; Fendorf, S. E.; Goldberg, S. *Environ. Sci. Technol.* **1998**, 32, 2383.

(123) Jain, A.; Raven, K. P. Loeppert, R. H. *Environ. Sci, Technol.* **1999**, 33, 1179.

(124) Uhlig, H. H.; Revie, R. W. *Corrosion and Corrosion Control*, 3rd ed.; John Wiley: New York, 1985.

(125) Pourbaix, M. *Atlas of Electrochemical Equilibria*; Pergamon Press: Oxford, 1966.

(126) Bard, A. J.; Faulkner, L. R. *Electrochemical Methods*; John Wiley: New York, 1980.

(127) *Test Methods for Evaluating Solid Waste*; U. S. Environmental Protection Agency, Office of Solid Waste: Washington, DC, 1986; EPA SW-846.

(128) Gregus, Z.; Gyurasics, A.; Csanaky, I. *Toxicological Sciences* **2000**, 56(1), 18.

(129) Bockris, J. O'M.; Reddy, A. K. N. *Modern Electrochemistry*; Plenum Press: New York, 1970.

(130) Talbot, D.; Talbot, J. *Corrosion Science and Technology*; CRC Press: Boca Raton, FL, 1998.

(131) Thiel, P. A.; Madey, T. E. *Surf. Sci. Rep.* **1987**, 7, 211.

(132) Cui, D.; Eriksen, T. E. *Environ. Sci. Technol.* **1996**, 30, 2259.

(133) Cui, D.; Eriksen, T. E. *Environ. Sci. Technol.* **1996**, 30, 2263.

(134) Hiemenz, P. C.; Rajagopalan, R. *Principles of Colloid and Surface Chemistry*, 3rd ed.; Marcel-Dekker: New York, 1997.

(135) Melitas, N.; Chuffe-Moscoso, O.; Farrell, J. *Environ. Sci. Technol.* **2001**, 35, 3948.

(136) Reardon, E. J. Environ. Sci. Technol. 29, 12, 2936.

(137) Gu, B.; Liang, L; Dickey, M. J.; Yin, X.; Dai, S. *Environ. Sci. Technol.* **1998**, 32, 3366.

(138) Qiu, S. R.; Lai, H. F.; Robertson, M. J.; Hunt, M. L.; Amrhein, C.; Giancarlo, L. C.; Flynn, G. W.; Yarmoff, J. A.; *Langmuir* **2000**, 16, 2230.